ANNUAL REPORT

October 1, 1969 - September 30, 1970

University of California, San Diego

National Aeronautics and Space Administration

Research Grant No. NGL 05-009-103

Principal Investigator: Norman A. Baily
Professor of Radiology

DISTRIBUTION:

5 Copies - National Aeronautics and Space Administration
Office of Scientific and Technical Information (Code US)
Washington, D.C. 20546

1 Copy - Dr. Leo Fox, Headquarters, NASA, OART,
600 Independence Avenue, S.W.
Washington, D.C. 20546

2 Copies - General Research Branch, NASA
Langley Research Center
Hampton, Virginia 23365

1 Copy - Mr. Sheldon Peterson, NASA Langley Research Center
Hampton,
Virginia 23365

INTRODUCTION

Although the research program supported by this grant is a cohesive one, with all aspects intended to focus on the central issue, for reporting purposes, it is more convenient to break it down into several sections. During the past year, research has been conducted in the following areas:

1. Experimental Physics (Microdosimetry). This program is designed to yield detailed physical information on:

   a) The distribution in size of the energy depositions representing single events (particle traversals) in volumes of biological significance when high energy charged particles cross such a volume.

   b) The spatial distribution of the secondary particles released by such events.

These have or will be looked at as a function of particle, energy, mass, and charge, the average atomic number of the medium it traverses, and the amount of such material traversed. To date, our effort has concentrated on effects of protons having energies of interest in manned space missions.

2. Theoretical Approaches to Microdosimetry. Sufficient basic physics data has been acquired so that the exact discrepancies from the two theoretical formulations can be identified. From our experimental data, we feel a good approximation to the actual distribution can be achieved by combining the Blunck-Leisegang corrected Vavilov formulation with an empirical formula describing the tail. The Kellerer formulation has too many variables to make use of this approach at this time. Until clarification is obtained on the exact form of the characteristic spectrum further comparisons cannot be made.

3. Radiobiology. No experimental work was carried out during this period. However, a detailed analysis of the implications for radiobiology of our physical data has been made. It would appear that this data implies that a serious reconsideration of many dosimetric and biological concepts is required.

4. Single-Scan TV. With the exception of gray level data output from the scanner, complete data on resolution and gray levels are available for the camera, camera plus video disc, and the camera-video-disc-electronic scan converter combination are now available. Combining of these with x-ray units and outputing the data to the computer is now in progress. Acquisition of a small laboratory computer will facilitate this portion of the program.

1. Experimental Physics (Microdosimetry).

During this past year, data on the frequency distribution of ~ 50 MeV protons has been acquired for pathlengths corresponding to pathlengths in tissue ranging from 0.24 μ to 240 μ. In addition, the influence of thin interfaces (~ 1 mm) of soft tissue (muscle) and of bone have been studied.

This work has been previously reported[1-3] and will not be described here. We have

---

1. Semi-Annual Report, October 1, 1969 - March 31, 1970, NASA, NGL 05-009-103, App. A.

2. N. A. Baily, J. E. Steigerwalt, and J. W. Hilbert: Phys. Rev. 2 B, 577 (1970).

3. Semi-Annual Report, October 1, 1969 - March 31, 1970, NASA, NGL 05-009-103, p. 1-4.

---

extended this work to shorter pathlengths and now have complete data for frequency distributions corresponding to tissue pathlengths of 0.24 μ, 0.48 μ, and 0.72 μ. For the shortest pathlength, the average energy deposited is $\approx$ 400 eV. Since this data was only recently acquired, computer processing is not yet complete. The experimental curves and their empirical fits to theory will be discussed in our next report.

During our last cyclotron run, two spectra were taken with the recently completed tissue equivalent cylindrical counter. At the lowest pressure that we have operated to date, the average energy of this distribution was $\approx$ 800 eV. It is planned to use this counter for investigations of particle beams having significant numbers of nuclear interactions. However, before we proceed with this portion of our research, further investigations of a tissue equivalent counting gas is required.

2. Theoretical Approaches to Microdosimetry.

As previously noted, the Blunck-Leisegang corrected Vavilov theoretical distribution predicts the general shape of the experimental results in the energy loss regions about the most probable. However, there is no agreement in the high energy loss region, a region which

influences, probably to a large extent, the mechanisms of biological damage and in the small energy loss region.

Theoretical methods which describe the experimental data are highly desirable, since radiobiological modeling potentially becomes much easier if the experimental frequency distributions can be predicted from theory even if only for some simple geometrical conditions. It is for this reason that we have explored in addition to the Vavilov theory Kellerer's[4] approach

---

4. A. M. Kellerer: Proc. of the Symposium on Microdosimetry, EVR 3747 d-f-e, 57 (1967).

---

to the problem.

Kellerer has pointed out that the primary collision spectrum (i.e. the cross-section for energy transfer) is the most influential factor in determining the shape of the energy loss distribution. The final energy loss distribution is obtained from the primary collision spectrum by a method called "The Compound Poisson Process." This method is used to describe the distribution of a random variable (energy loss) when it is composed of independent events (electron collisions) of variable size (energy loss/collision). The number of events which takes place is subject to Poisson statistics, and the resulting event size distribution is a function of the energy transfer cross-section, $w(\epsilon)$. This cross-section is then called the characteristic spectrum of the Poisson Process. The basic operation which is done is called convolution, since the solution to larger mean energy losses is obtained by convolution of $w(\epsilon)$. $w(\epsilon)$ is normalized to correspond to exactly one collision of the particle in passing through the pathlength. The solution to the case where exactly two collisions are made along the pathlength is given by the integral

$$w^{*2}(\Delta) = \int_0^{\Delta} w(\Delta - \epsilon)\, w(\epsilon)\, d\epsilon$$

The same procedure can be extended for the situation when n collisions occur. This gives

$$w^{*n}(\Delta) = \int_0^{\Delta} w^{*n-1}(\Delta - \epsilon)\, w(\epsilon)\, d\epsilon$$

If $\overline{\Delta}$ is the mean energy loss in the proportional counter, and $\overline{\epsilon}_1$ is the mean of $w(\epsilon)$, then the distribution of energy losses in the proportional counter, $f(s, \Delta)$, is given by

$$f(s, \Delta) = \sum_{\nu=0}^{\infty} e^{-\overline{\Delta}/\overline{\epsilon}_1} \left(\frac{\overline{\Delta}}{\overline{\epsilon}_1}\right)^{\nu} \frac{1}{\nu!}\, w^{*\nu}(\Delta)$$

This expression can be understood as the sum over all possible collision numbers, ν, of the Poisson probability of ν collisions occurring times the probability that exactly ν collisions will produce an energy loss Δ. An alternate approach is to look at the distribution of energy losses when, on the average, one or less, collisions are made along the pathlength. If we call this distribution $f_1(s, \Delta)$,

$$\text{then} \quad f_1(s, \Delta) = \sum_{\nu=0}^{\infty} e^{-\overline{\Delta}/\overline{\epsilon}_1} \left(\frac{\overline{\Delta}}{\overline{\epsilon}_1}\right)^{\nu} \frac{1}{\nu!}\, w^{*\nu}(\Delta)$$

$$\text{with:} \quad \frac{\overline{\Delta}}{\overline{\epsilon}_1} = 1; \qquad f_1(s, \Delta) = \sum_{\nu=0}^{\infty} e^{-1} \frac{1}{\nu!}\, w^{*\nu}(\Delta)$$

If one looks at the solution where, on the average, the number of collisions made is $\ll 1$, then one can approximate the solution by including only the leading term in the sum. Thus, a convolution of this solution, the appropriate number of times ($N = \overline{\Delta}/\overline{\epsilon}_1$) will give the desired energy loss distribution. This method has the advantage of avoiding carrying along terms from different convolutions of $w(\epsilon)$, and the final convolution is in fact the solution. As far as practical calculations are concerned, the successive distributions are convoluted into themselves, and thus, the number of convolutions needed, η, is given by $2^{\eta}\overline{\epsilon}_1 = \overline{\Delta}$.

Now the question arises as to the proper form of the characteristic spectrum $w(\epsilon)$. The form of $w(\epsilon)$ is theoretically very difficult to derive and there are only a few experimental results describing some portions of its shape. Classically, $w(\epsilon)$ follows a $1/\epsilon^2$ dependence.

FIG. 1: Comparisons of experimental data with theoretical formulations of energy loss frequency distributions. For each set of curves A is the experimental data; B is a Blunck-Leisegang corrected Vavilov distribution; and C is computed by Kellerer's method. The low energy group corresponds to a pathlength of 1.33×10^{-4} g/cm^2 tissue, the medium energy group to 6.66×10^{-4} g/cm^2, and the high energy group to 1.33×10^{-3} g/cm^2.

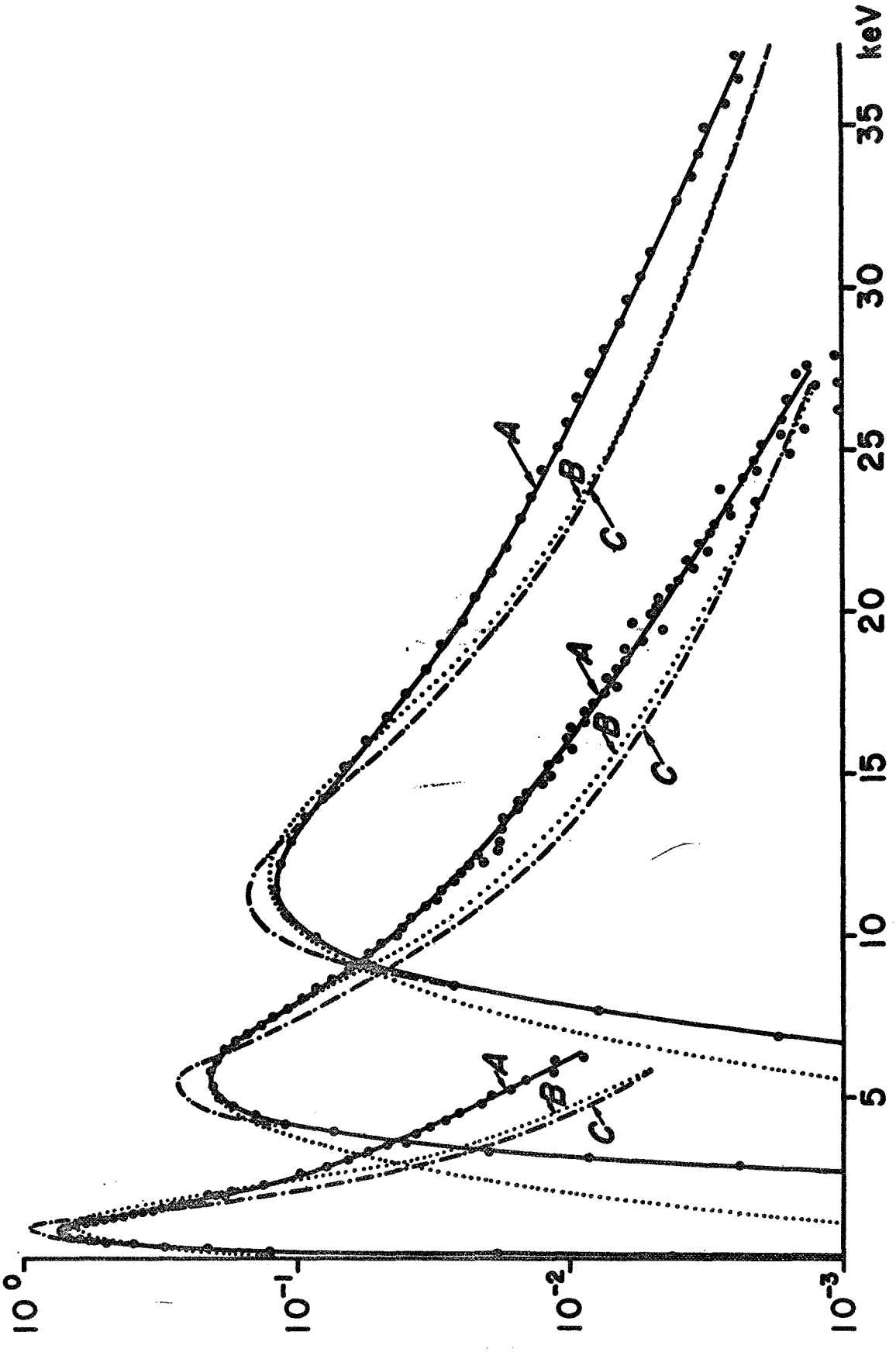
PROB/keV
10^{0}
10^{-1}
10^{-2}
10^{-3}
5
10
15
20
25
30
35
keV
A
B
C
A
B
C
A
B
C

The stopping power is obtained from the following integral:

$$\frac{dE}{dx} = \int_{\epsilon_{min}}^{\epsilon_{max}} \epsilon w(\epsilon) d\epsilon$$

Obviously, such a form for $w(\epsilon)$ is only approximate. Kellerer has taken experimental values of $w(\epsilon)$ at low energies (actually, from energy loss of electrons), and used a $\frac{1}{\epsilon^2}$ dependence at energies greater than a few hundred eV, and then adjusted the function in between these limits such that the correct value of stopping power is obtained. He then developed a program that convolutes this primary spectrum from very low average collision numbers, to the collision number which corresponds to the desired solution.

We have formulated a characteristic spectrum applicable to 46.4 MeV protons and have used Kellerer's convolution program to obtain theoretical distributions for the pathlengths used in our experiments. Fig. 1 shows three sets of three curves each. For each set (A) is the Experimental Data; (B) is the Blunck-Leisegang corrected Vavilov Distribution; and (C) is Kellerer's Distribution. All theoretical curves have been modified to include corrections for counter resolution and noise broadening. The low energy group is for a pathlength of 1.33×10^{-4} g/cm^2, the medium energy group for a pathlength of 6.66×10^{-4} g/cm^2, and the high energy group corresponds to a pathlength of 1.33×10^{-3} g/cm^2. The points to note are as follows:

a) The Blunck-Leisegang corrected Vavilov distribution shows discrepancies with the data in both low and high energy loss regions but agrees well with the region about the most probable energy loss.

b) Both theoretical curves agree well with each other for high energy loss regions, probably a consequence of the $1/\epsilon^2$ assumption of both theories.

c) Kellerer's distribution agrees well with the data for low energy losses but shows discrepancies in regions about the most probable energy loss and for high energy losses.

It might be mentioned that by arbitrarily adjusting the assumed characteristic spectrum in the region between 100 - 1000 eV, keeping the value of the stopping power constant, Kellerer's solution can be brought in better agreement with the data for the region around the most probable energy loss with little change of shape for the tail.

There are two aspects of the problem which we have not considered in detail. That is, the possibility of energetic delta rays escaping from the proportional counter after having left only a portion of their energy in the sensitive volume and the contributions to the signal by forward and backward scattered electrons from the windows. This problem would require a major theoretical effort to even solve it approximately, and it appears almost impossible to compute this for a practical situation. Kellerer's approach to the problem, however, includes a method whereby the delta particle escape contributions can be approximately included. All that must be done is to modify the characteristic spectrum to exclude the delta ray energy that escapes. This approximation does not include extra contributions from electrons scattered into the sensitive volume; however, under the simple assumption of electronic equilibrium obtaining in the counter, one still keeps the stopping power the same but calculates the contributions to the stopping power from different energy regions of the collision cross-section. By using this artifice of including scattered contributions to the energy loss distributions in the collision cross-section, one hopes to produce theoretical spectra with some degree of validity. That this result is true, however, is not obvious and can only be of use if there is a consistent agreement between these theoretical curves and experiment for different sizes and shapes of sensitive volumes when the scattered contributions are calculated in a consistent way. If the condition of electronic equilibrium did not hold and one allowed only for the escape of delta rays, then the results of Kellerer's theory would not be reasonable when compared with the experimental results; i.e., the theoretical

FIG. 2: Frequency distributions in tissue for ~ 50 MeV protons. In each group, curves A show the experimental data; B a Kellerer distribution including delta ray energies up to E_{max} (~103 KeV); and C the Kellerer distribution modified to compensate for delta rays having ranges greater than the counter dimensions. The low energy group is for a pathlength of 1.33×10^{-4} g/cm^2, the medium energy for 6.66×10^{-4} g/cm^2, and the high energy for 1.33×10^{-3} g/cm^2 tissue.

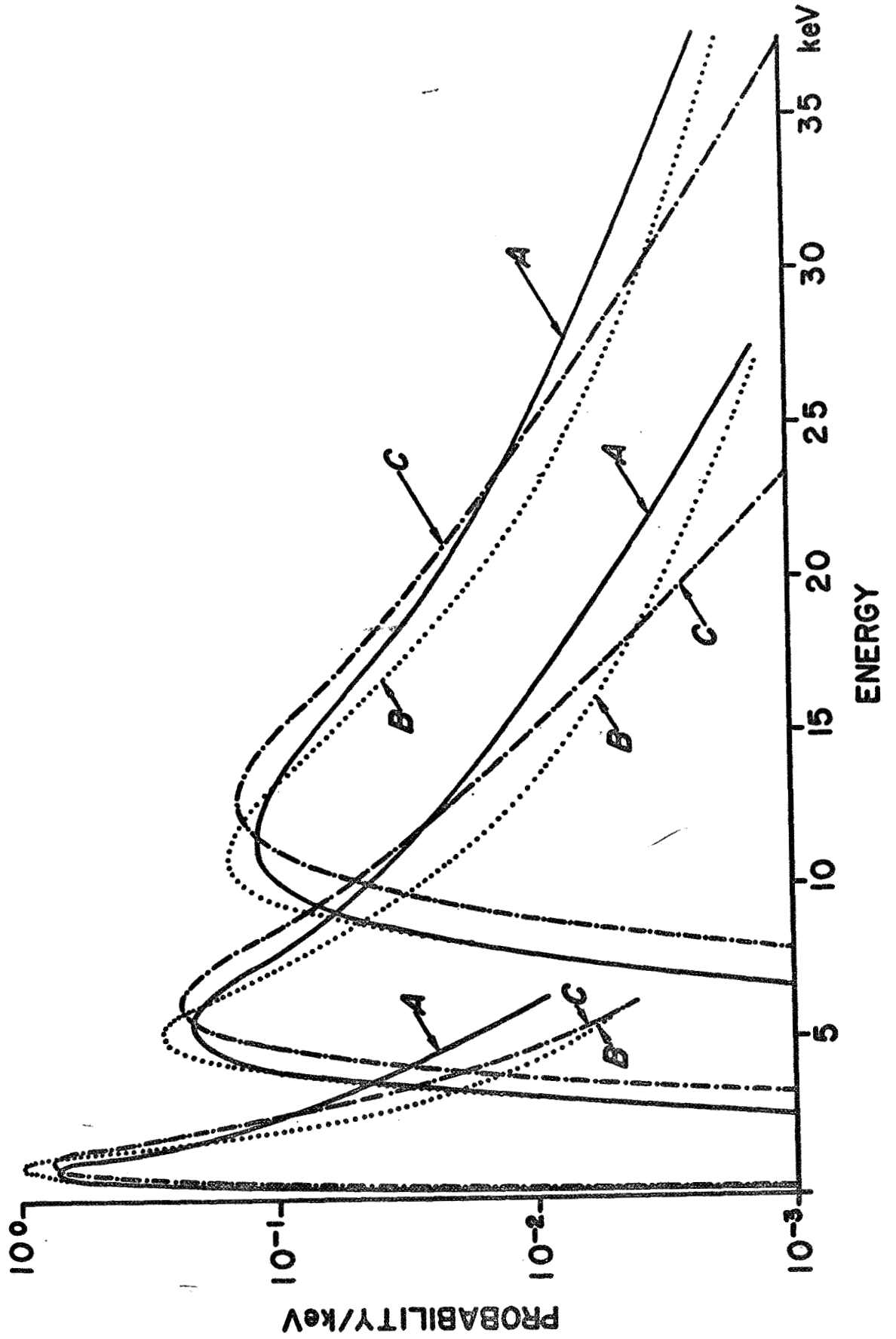
PROBABILITY/keV
10^{0}
10^{-1}
10^{-2}
10^{-3}
5
10
15
20
25
30
35 keV
ENERGY
A
B
C
A
B
C
A
B
C

curves drop off so rapidly so that they would approach a Gaussian shape and revert back to previous and erroneous concepts. Fig. 2 shows the experimental data and Kellerer's results using such modified characteristic spectra. The modification attempted to take into account electrons having ranges greater than the counter dimensions. In this figure, curves labeled A are the experimental data, and those labeled B are curves generated using Kellerer's formulation and an unmodified characteristic spectrum, while C represents an attempt to incorporate delta ray losses into the characteristic spectrum. The three groups represent the same pathlengths as shown in Fig. 1. The theoretical distribution does show some tendency to better agreement in the high energy loss regions but at the expense of poorer agreement in the other energy loss regions. This is probably due to the very simple choice of the form of the modification of the characteristic spectrum. Another major difficulty is the dependence of the most probable energy loss on the choice of characteristic spectrum. Our attempts to incorporate delta ray losses and scattered contributions into the theory do not give us any encouragement to continue this method.

It appears that Kellerer's approach shows promise only if (a) a detailed knowledge of delta ray escape probabilities; (b) window scattering contributions are known; and (c) the correct characteristic spectrum is used. These indeed are not trivial and possibly preclude verifying this theory with experimental results. This is particularly the case for biological geometries. A further difficulty would be that one would need a different characteristic spectra for each pathlength or geometrical configuration investigated. A procedure which is not very satisfactory would be to find by trial and error the form of each characteristic spectrum which yielded the experimental curves and hope to find some generalizations in the shapes of these functions, then one would be able to predict a new characteristic function for each new pathlength. Although we will continue to investigate correlations between theory and experiment, it now appears more firmly than ever that the only feasible

approach to a solution is through acquisition of a sufficient amount of experimental data. However, the spectra obtained to date will be used to check the Kellerer method further.

What then of the possibility of finding a method to derive the correct form of the characteristic spectra from the experimental results? The approach would have to involve a process of deconvolution of the experimental curves. At the moment, no program such as this exists which could reliably extract the characteristic spectrum. A major attempt to produce such a program would probably not be advisable since the solution to this type of problem is subject to large oscillations which originate from the statistical spread in the experimental data.

The best attempt thus far has been produced by Kellerer and consists of a program to deconvolute an experimental spectrum to arrive at distributions which have their mean energy in a limited region around the mean energy of the initial distribution. This method of deconvolution uses the Fast Fourier Transform calculation. A factor of two seems to be about the largest that one can shift the mean of the deconvoluted distribution from the initial distribution and still obtain reasonable results. The accuracy of the result is still subject to the smoothness of the initial distribution. If this approach shows promise, then one has a procedure which would be very useful for an empericial method of generating such distributions.

Since deconvoluting a distribution to arrive at a desired spectra seems to agree better with experiment than convolution of an alternate distribution, the procedure to test this approach will be to deconvolute the 1.33×10^{-4} g/cm^2 distribution, through the intermediate spectra corresponding to 8.87×10^{-5} g/cm^2 (0.72 μ) and 6.66×10^{-5} g/cm^2 (0.48 μ) and then to compare it with the 3.33×10^{-5} g/cm^2 (0.24 μ) spectra. In this way, the deconvolution limits on the average energy are kept within a factor of two, and all intermediate results can be experimentally checked. One hopes then to determine to what extent this method can be used to predict experimental spectra and what limits should be considered. These calculations are now in progress.

This way, delta ray losses and scattered contributions could be handled in a natural way.

For instance, the energy loss distributions obtained from the proportional counter reflect the distributions with delta ray losses and with scattered contributions included. The idea then is that one could arrive at solutions for the energy loss distribution corresponding to an arbitrary mean energy loss but using as a starting point, the empericial energy loss distribution having some known mean energy. There would be a certain ambiguity in the results, however, since the delta ray loss distributions and the scattered contributions vary as the mean energy loss varies. Hopefully, if the mean energy loss considered is close enough to that started with, this ambiguity will be of secondary importance in the resulting energy loss distribution. One would thus be freed from the requirement of finding the correct form of $w(\epsilon)$ and would still be able to generate the solutions $f(\Delta, s)$ for arbitrary $\bar{\Delta}$ provided one had an empericial solution for the distribution with mean energy loss $\bar{\Delta}_o$. We have preliminary results that indicate that the solutions converge generally, provided that $\bar{\Delta} \leqslant 2\bar{\Delta}_o$ or $\geqslant \frac{\bar{\Delta}_o}{2}$.

For composite energy loss distributions suitable for applications to arbitrary biological volumes the functions $f(\Delta, Si)$ must be found for the pathlengths, Si, which are characteristic of the biological volume. Thus, the empericial spectra which must be obtained should be chosen to span the energy loss regions corresponding to the Si. These spectra can be taken with sufficient care and for a sufficient length of time that adequate statistics are accumulated in the high energy tail and the deconvolution program would then have an easier time in converging to a solution.

3. Radiobiology.

Although it has been known for many years that the loss of energy by a charged particle in its passage through matter is subject to wide fluctuations[5-7], this fact has been largely ignored

---

5. L. Landau: J. Phys. USSR 8, 201 (1944).

6. P. V. Vavilov: Zh. Eksperim. i. Teor. Fiz. 32, 320 (1957) English Transl.: Soviet Phys. - JETP 5, 749 (1957).

7. O. Blunck and S. Leisegang: Z. Physik 128, 500 (1950).

---

by investigators concerned with the biological effects of ionizing radiation. Much attention has of course been paid to the quantity known as LET and to systems of microdosimetry designed to illucidate this quantity. What has been largely ignored is the fact that when the energy lost in the volume of interest is small compared to the particle energy, the fluctuations in energy loss are so great as to make average values (LET) rather meaningless. This fact holds whether the charged particle is a portion of the primary beam, a secondary electron generated by a primary photon, or secondary charged particles generated by a neutron beam. In the past few years, Baily and his collaborators[2, 8, 9] have shown that (1) despite certain

---

8. J. W. Hilbert, N. A. Baily, and R. G. Lane: Phys. Rev. 168, 290 (1968).

9. J. W. Hilbert and N. A. Baily: Rad. Res. 39, 1 (1969).

---

discrepancies from the theoretical predictions, a rather good picture of energy loss in small volumes can be obtained by calculation; (2) the fluctuations in energy loss in many cases will be large enough to invalidate the concepts of LET and average energy loss (dose on a cellular level); (3) the most probable energy loss is significantly different than the average or mean energy losses. Such measurements have, therefore, thrown much doubt on the validity of published values of RBE, inactivation cross-sections, etc.

The fluctuations in energy loss by a charged particle traversing matter become more and more significant as its energy (velocity) increases and its pathlength in the volume under consideration becomes smaller. This becomes particularly significant when models or calculations make use of such concepts as a minimum energy required for damage[10], damage in individual

---

10. R. Katz: Proc. of the 3rd Int. Cong. of Rad. Res., Evian, France (1970).

---

cells or molecules[11], and calculations based on numbers of traversals calculated from stopping power theory[12].

---

11. G. W. Barendsen, H. M. D. Walter, J. F. Fowler, and D. K. Bewley: Rad. Res. 18, 106 (1963).

12. A. H. Sullivan: Health Phys. 14, 299 (1968).

In those instances where a charged particle makes many collisions in the volume of interest and the total energy lost within that volume is large compared to the particle energy, the distribution of energy lost per event will essentially be a delta function at $\bar{E}$ the average energy loss as computed from the stopping power of the particle for a particular material. Dosimetric calculations, biological cross-sections, etc. have mainly been treated from this viewpoint. Although it has been pointed out by many authors that the loss of energy to ionization by collisional processes is in reality a discontinuous process, it has been tacitly assumed that this approximation was warranted. It was reasoned that the statistical spreading would at worst produce a Gaussian spread in the distribution of the energy lost per event with such spreads having a rather narrow FWHM (full width at half maximum) about the average energy loss. In fact, however, for volumes of biological interest, these distributions assume a rather large spread[2] and further have a most probable energy loss which can be considerably lower than the average. In such cases then, a majority of events occur with energy losses lower than would be expected either from calculations using the stopping power or from measurements of absorbed dose.

THEORY

The Blunck-Leisegang[7] corrected Vavilov[6] distribution can be expressed as[13]

---

13. U. Fano: Ann. Rev. Nucl. Sci. 13, 1 (1963).

$$f(X, \Delta) = \frac{1}{\sqrt{\pi}\, b\, \xi} \int_{-\infty}^{\infty} f_L(X, \Delta')\, e^{-\frac{(\Delta - \Delta')^2}{\xi^2 b^2}}\, d\Delta' \qquad (1)$$

where: $f_L(X, \Delta')$ = Vavilov Distribution

b = Blunck-Leisegang Parameter

$$\xi = \frac{2\pi N_o z^2 e^4}{mv^2} \frac{Z}{A} X$$

N_o = Avagadro's Number

X = Pathlength $\left[gm/cm^2\right]$

Z = Atomic Number of Medium

A = Atomic Weight of Medium

$v = \beta c$ = Velocity of Incident Particle

z = Charge of Incident Particle

In can be shown that: $$\bar{\Delta} - \Delta_{mp} = \xi\,(-0.4228 - \beta^2 - \lambda_{max} - \ln \kappa) \qquad (2)$$

where: Δ_{mp} = Most Probable Energy Loss

λ = Landau Parameter

$$\kappa = \frac{\xi}{\Delta_{max}}$$

Δ_{max} = Maximum Energy Transfer which the charged particle can give to an atomic electron.

The value of λ_{max} can be obtained from plots of the distribution function given by Equation (1).

It will be seen from examination of Equations (1) and (2) that the spread of the distribution function (FWHM) and the degree of difference between the most probable energy loss and the average energy losses are functions of several parameters. These are first of all a function of the material parameters; namely, the electron density and the pathlength of the medium being traversed. If these remain constant, then the two parameters of interest are

FIG. 3: Fraction of the total energy delivered by a 46.4 MeV proton traversing 1.33×10^{-4} g/cm^2 tissue delivered in events of a size greater than a given energy.

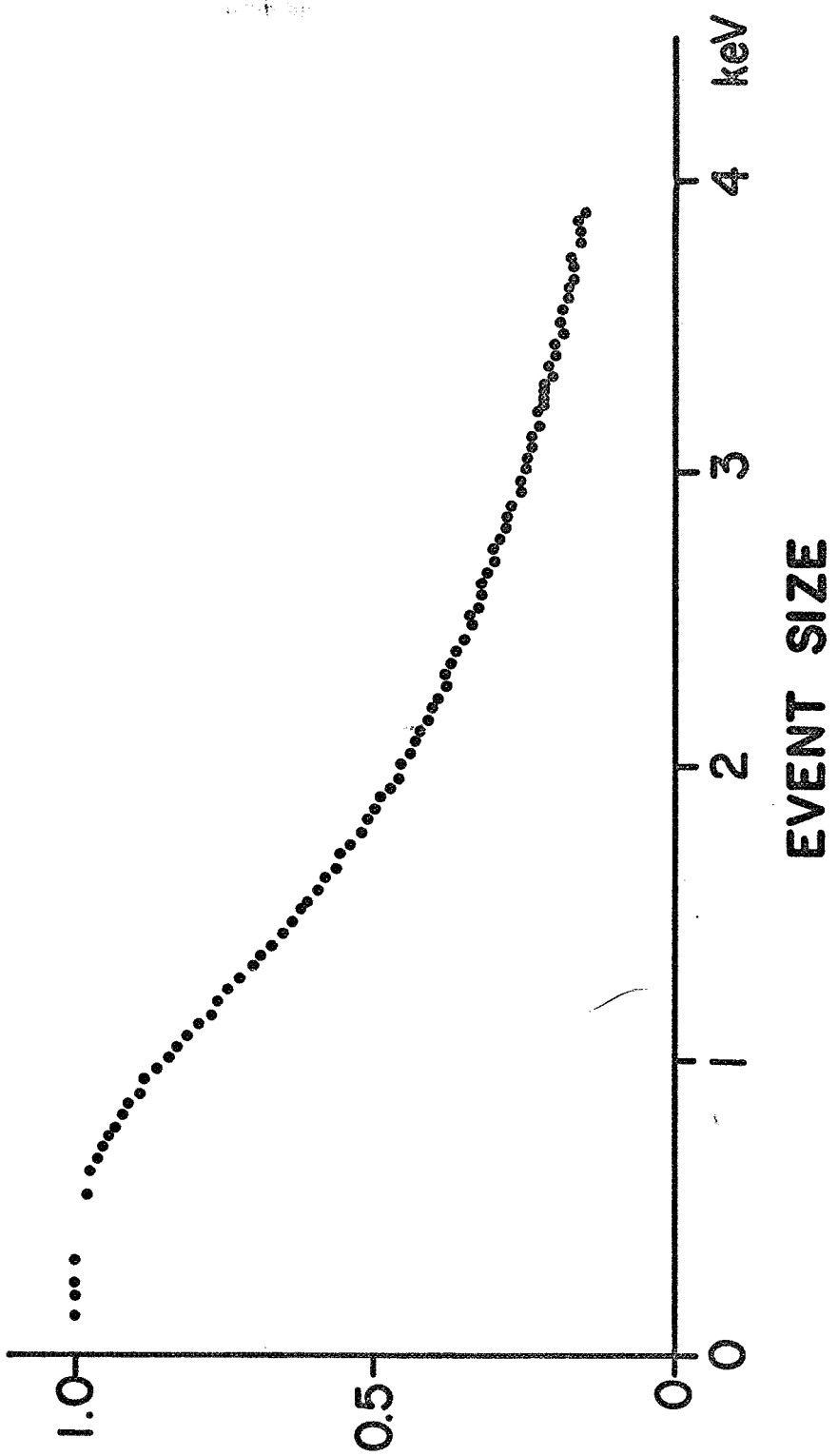
FRACTION OF
TOTAL ENERGY DEPOSITED
ABOVE A GIVEN SIZE EVENT
1.0
0.5
0
0
1
2
3
4 keV
EVENT SIZE

FIG. 4: The fraction of energy transfers above any given energy that occur in a pathlength of 1.33×10^{-4} g/cm^2 tissue from a proton of energy equal to 46.4 MeV.

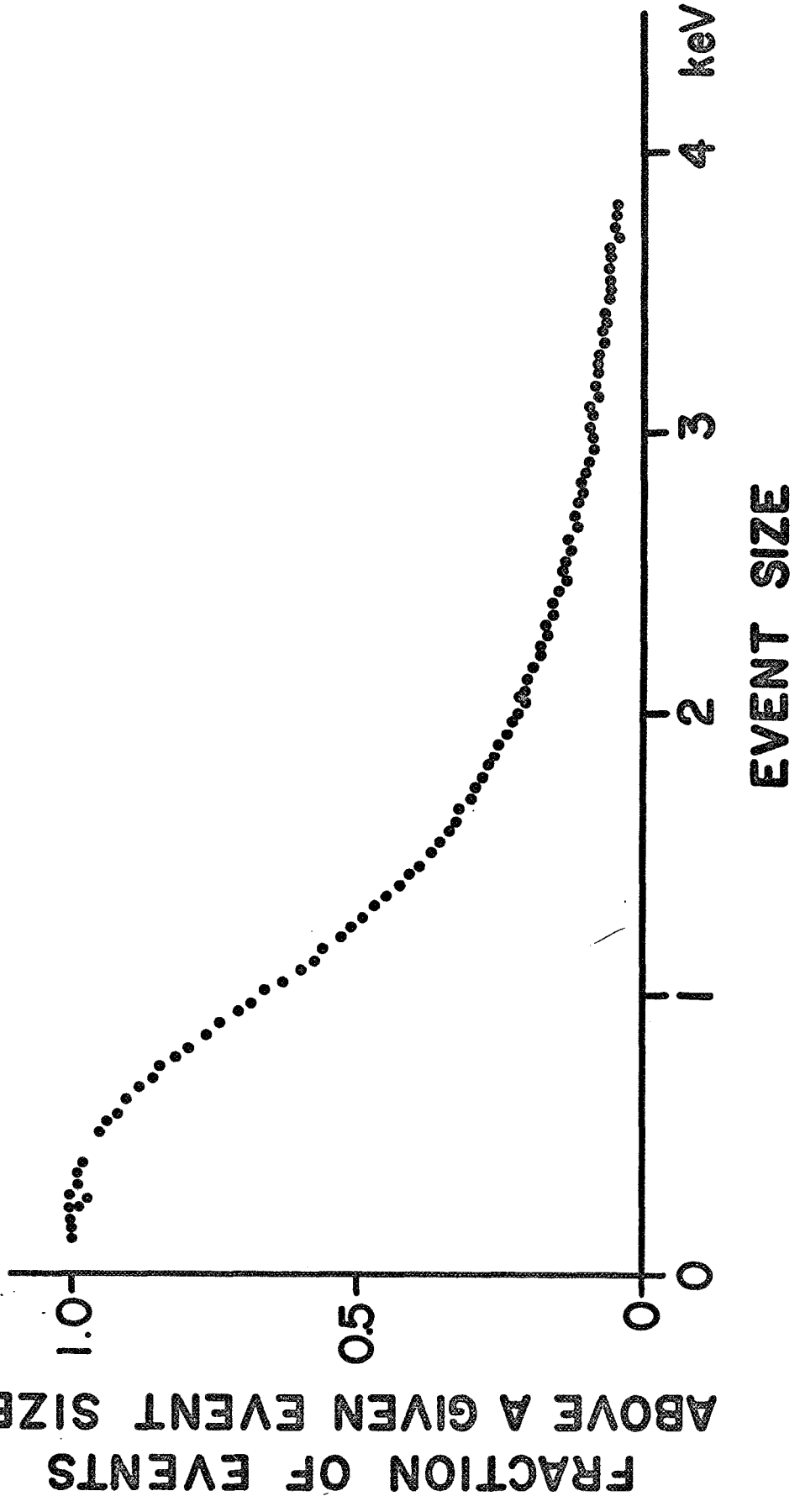
FRACTION OF EVENTS
ABOVE A GIVEN EVENT SIZE
1.0
0.5
0
0
1
2
3
4 keV
EVENT SIZE

TABLE I

ENERGY LOSS PARAMETERS FOR PROTON PASSAGE THROUGH 1 μ TISSUE

Proton Energy (MeV)	$\overline{\Delta}$, Average Energy Loss (KeV)	Δ_{mp}, Most Probable Energy Loss (KeV)	$\overline{\Delta} / \Delta_{mp}$
1.0	35.15	36.19	0.971
1.5	26.32	25.54	1.031
2.0	21.23	20.06	1.058
3.0	15.65	13.73	1.140
4.0	12.55	10.51	1.195
5.0	10.55	8.409	1.255
6.0	9.140	7.063	1.294
8.0	7.268	5.358	1.356
10.0	6.078	4.332	1.403
15.0	4.379	2.946	1.486
20.0	3.466	2.245	1.544
30.0	2.493	1.537	1.622
40.0	1.976	1.173	1.685
50.0	1.653	0.958	1.725
100	0.967	0.525	1.842
150	0.722	0.379	1.905
300	0.467	0.233	2.004
600	0.338	0.163	2.074

TABLE II

ENERGY LOSS PARAMETERS FOR ELECTRON PASSAGE THROUGH 1 μ TISSUE

Electron Energy (MeV)	$\bar{\Delta}$, Average Energy Loss (KeV)	Δ_{mp}, Most Probable Energy Loss (KeV)	$\bar{\Delta}/\Delta_{mp}$
0.1	0.4154	0.1980	2.098
0.2	0.2817	0.1250	2.254
0.4	0.2164	0.0915	2.365
0.6	0.1976	0.0824	2.398
0.8	0.1902	0.0790	2.408
1.0	0.1869	0.0778	2.402
2.0	0.1866	0.0795	2.347
4.0	0.1950	0.0860	2.267
6.0	0.2026	0.0911	2.224
8.0	0.2094	0.0950	2.204
10.0	0.2158	0.0981	2.200

controlled by the particle's velocity and charge. The spread in the distribution function and the percentage difference between the most probable and the average energy losses both increase with increasing particle energy, that is, its velocity and with decreasing pathlength in the medium.

Although some discrepancies between experiment and theory[2] seem to exist, the experiments to date bear out the overall correctness of the theory and the importance of the magnitude of these factors on biological effects.

EXAMPLES

Another way of looking at the data presented by Baily, et al.[2] is to plot the fraction of the total energy delivered by events above a given energy and the fraction of events occurring with energies above a given energy. Two such curves are shown in Figs. 3 and 4. These curves are for protons having kinetic energies of 46.4 MeV and pathlengths in a tissue equivalent gas of 1.33×10^{-4} g/cm^2. In one case, the fraction of total energy delivered to the sensitive volume in event sizes greater than $\bar{\Delta}$(1.56 KeV) is 60%, while the fraction delivered by events having energy losses greater than Δ_{mp} (0.90 KeV) is 88%. In the other case, the fraction of events occurring with energy losses greater than $\bar{\Delta}$is only 35%, while that occurring with losses greater than Δ_{mp} is 73%.

It is also of interest to examine the difference between Δ_{mp} and $\bar{\Delta}$as a function of particle type and energy.

Tables I and II give for protons and electrons respectively the average energy loss, the most probable energy loss, and the ratio of the two for some particle energies of interest.

DISCUSSION

In the usual range of interest, it is seen that for protons the difference between the average energy loss and the most probable energy loss becomes of greater importance as the

proton energy increases. However, the case with electrons is distinctly different, since radiation losses become significant at moderate energies and the maximum energy transfer continues to increase. It is interesting to note that the effect with which we are concerned is most significant in the energy range most frequently used for biological experiments and radiation therapy. Indeed, even where γ and x-rays are used, large numbers of Compton electrons are generated in this energy range thereby making some consideration of the spread in energy deposition significant.

Consideration of this physical factor in the energy deposition pattern is required, since all radiobiology is based on theories requiring only a small number of so-called hits in the sensitive volume. It is evident then, that use of the average energy loss is incorrect and if for convenience sake one wants to talk about one specific energy, the most probable energy loss would be a more realistic value. However, it would appear that for consideration of a single-cell, a chromosome, etc., one must take into consideration the statistical distribution of energy losses at least in those cases where the spread of energy losses is significant. The averaging over large numbers of cells does not affect this consideration, since the damage incurred by the passage of a particle through a critical volume is a function of the energy deposited therein, if our present concepts of radiobiology are valid.

Similarly, those calculations for sensitive volume size utilizing average energy loss, or LET, would be in error in the cases simulated.

The tables given are presented for illustrative purposes only. If as suspected by many people[10, 12], the sensitive sites are smaller than cellular dimensions, the effect discussed is of even greater significance since the skewness of the distribution increases as the ratio of average energy loss to particle energy decreases.

CONCLUSIONS

1. The importance of the spread and skewness of the frequency distribution of energy loss

events in small volumes by fast charged particles has not been taken into account when models of radiobiological damage have been discussed. In fact, the use of LET would appear to lead to erroneous concepts. The use of the parameter z^2/β^2 [10, 12] would appear to be consistent with our concepts since this parameter also defines the parameter ξ. However, use of this fraction alone still ignores the statistical nature of the energy deposition pattern.

2. For both protons and electrons at energies of current interest, both the magnitude of the FWHM and the large difference between average and most probable energy losses are probably significant factors and warrant consideration for radiobiology, radiation protection, and radiation therapy.

4. Single-Scan TV.

The installation of one x-ray unit (Basic Science Building) is now completed and the second unit at the University Hospital is scheduled for completion during October of this year. Installation of the single-scan system will be accomplished on both units within the next three months. A computer program for handling the digitized data has been written and tested. This will allow immediate use and testing of the complete system.

SPECIFIC TESTING

Initial attempts to determine the Modulation Transfer Function (MTF) of the MVR video disc recorder were hampered by modulation/demodulation distortions inherent to the video disc. These distortions appeared as amplitude modulation of the output of the video disc. This amplitude modulation was more prominent at some frequencies, particularly those lying near the carrier frequency of the video disc (adjustable between 4.0 and 5.0 MHz). The effects of the distortion of the high frequencies corresponding to high spatial frequencies was brought within tolerable levels by raising the frequency of the modulator of the disc to the highest practical frequency of operation. Additionally, the amount of negative feedback

FIG. 5: Output (composite video signal) of Cohu Model 3201-11 TV - Camera. This response is for a single horizontal line.

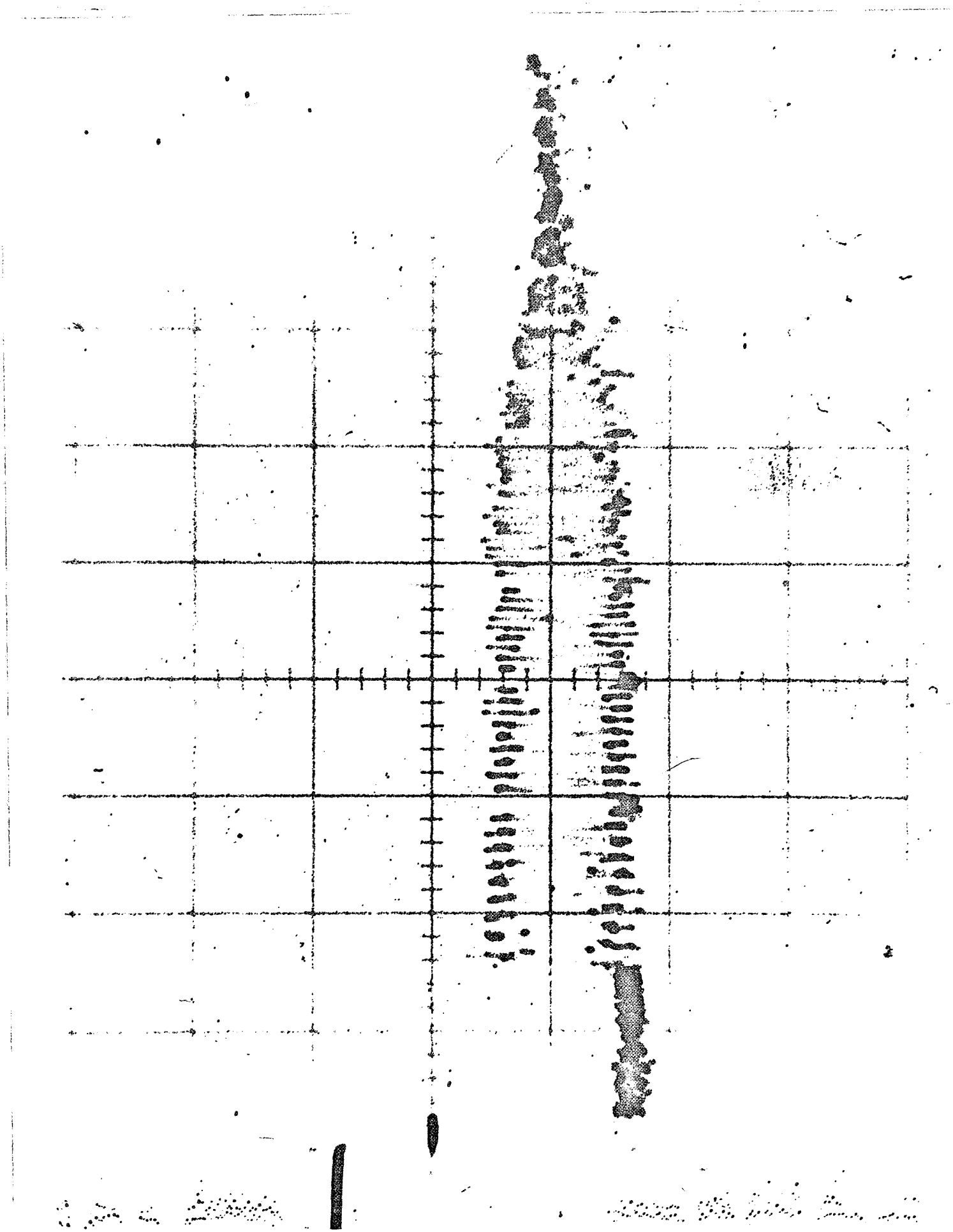

FIG. 6: Output (single horizontal line) of TV-Camera-Video Disc combination.

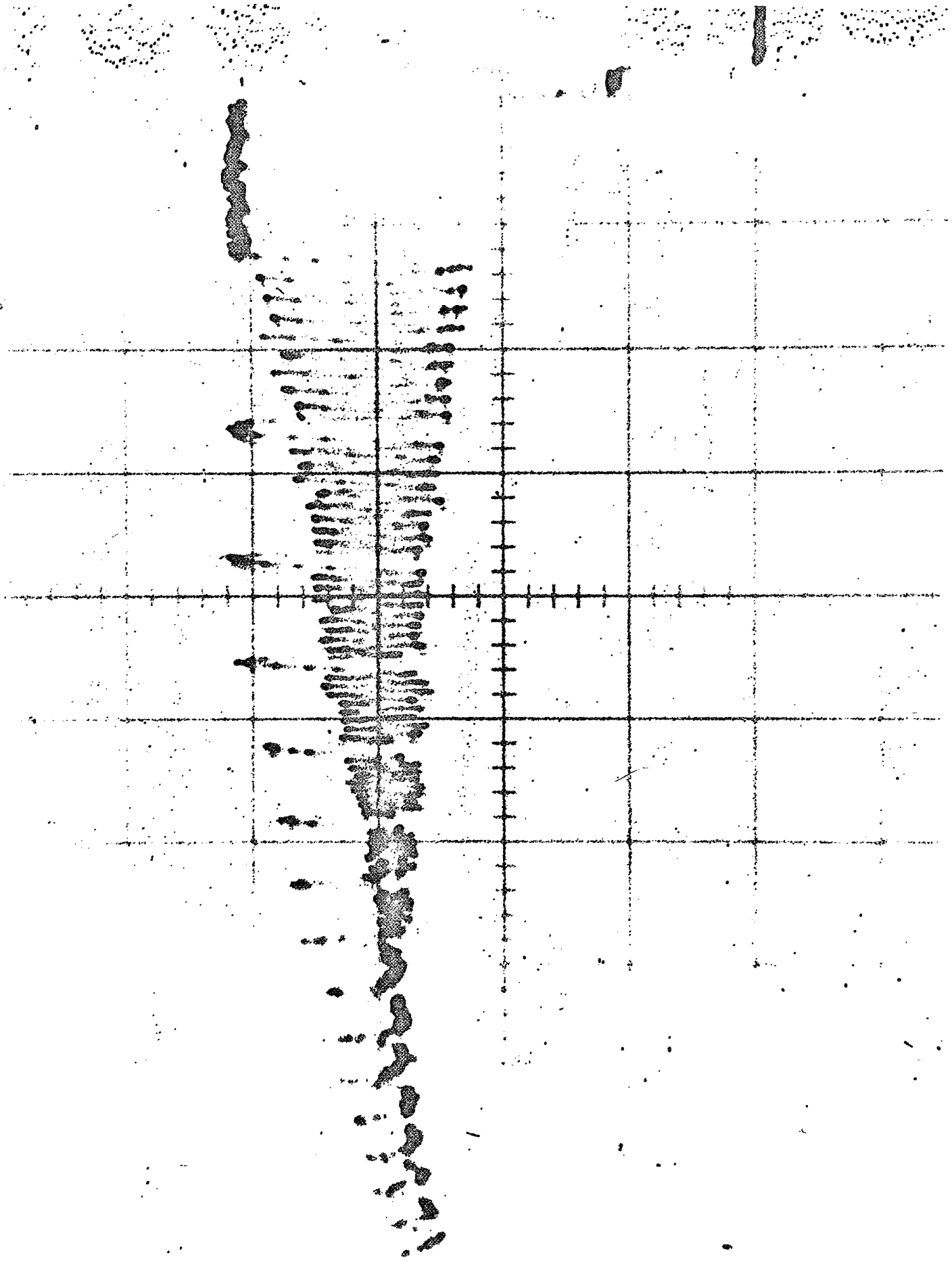

FIG. 7: Modulation Transfer Function for a single horizontal scan line of TV Camera-Video Disc combination when operated in usual video mode (double field).

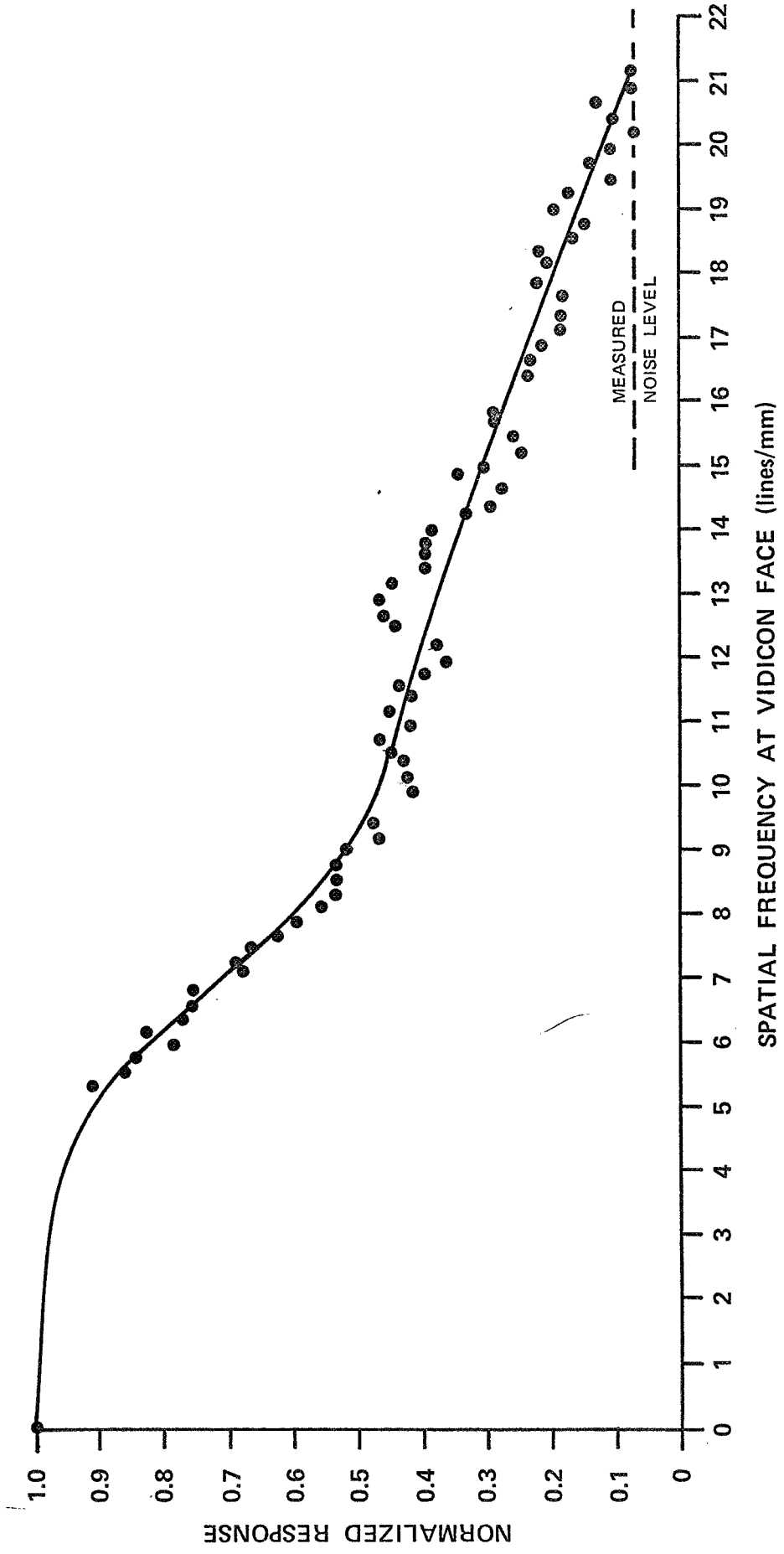
NORMALIZED RESPONSE
1.0
0.9
0.8
0.7
0.6
0.5
0.4
0.3
0.2
0.1
0
0 1 2 3 4 5 6 7 8 9 10 11 12 13 14 15 16 17 18 19 20 21 22
SPATIAL FREQUENCY AT VIDICON FACE (lines/mm)
MEASURED
NOISE LEVEL

FIG. 8: Response of Cohu TV Camera to Gray Wedge.

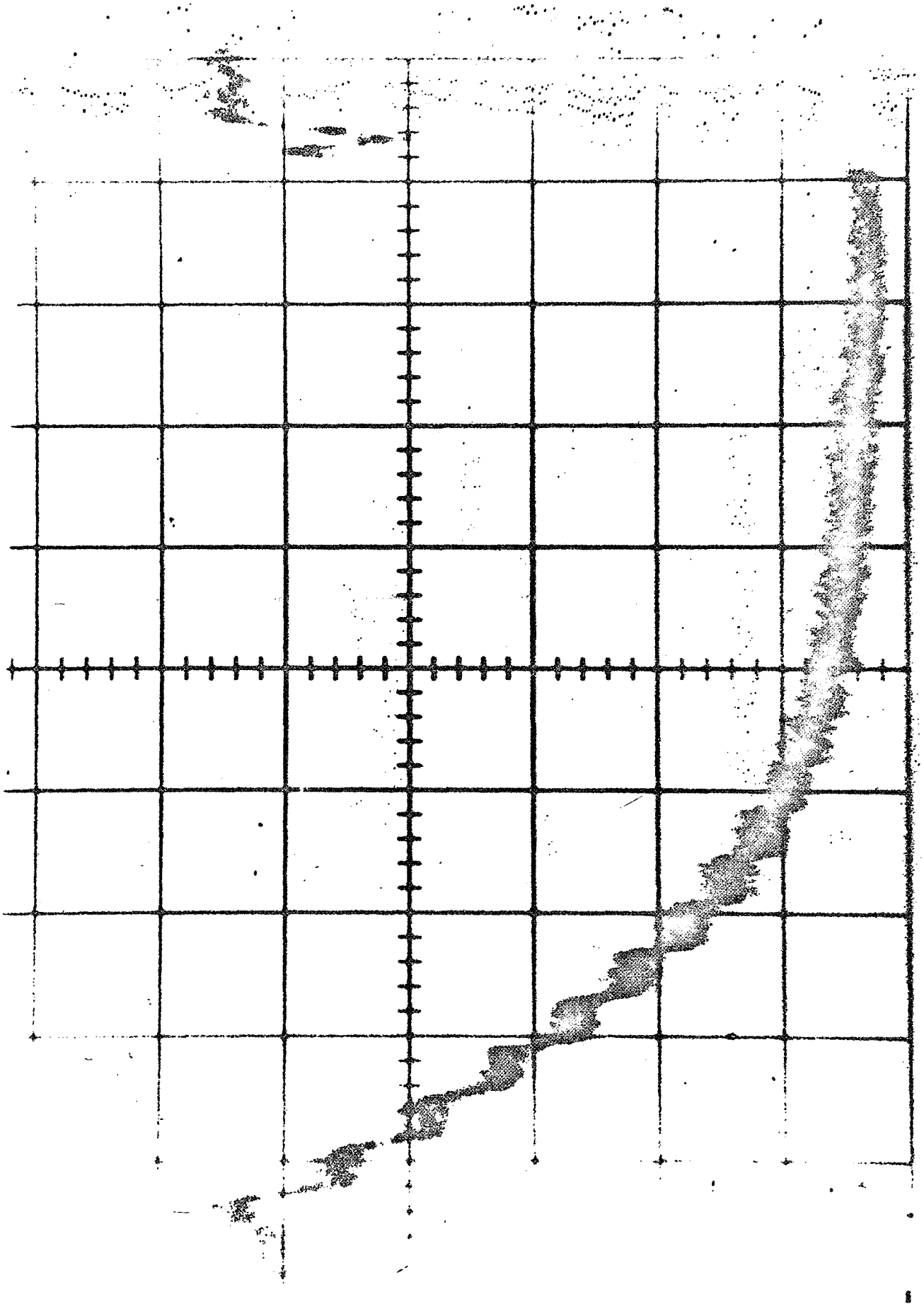

FIG. 9: Response of Video-Disc to Gray Wedge Input.

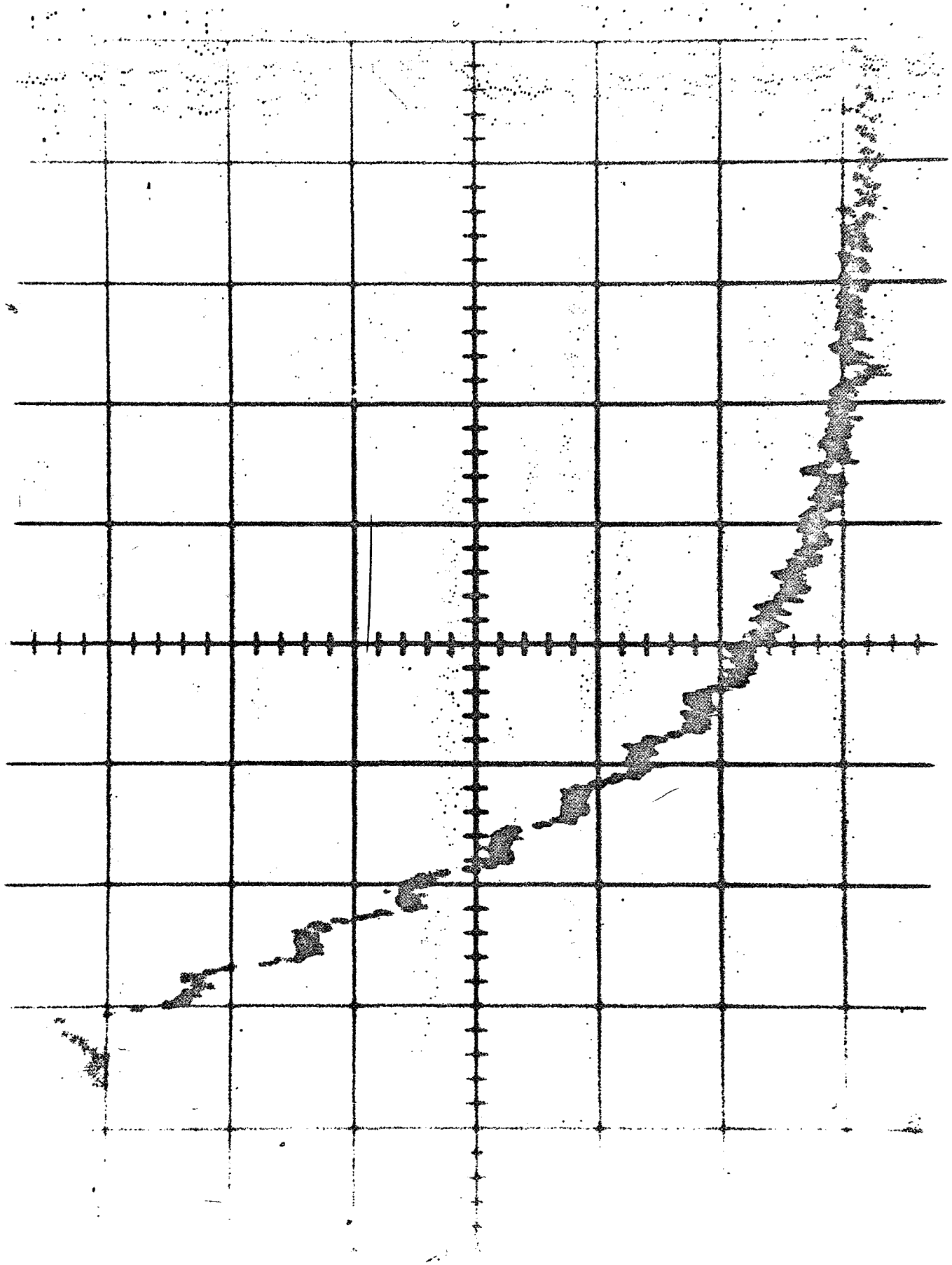

FIG. 10: Relative responses of TV Camera, Video Disc Electronics, and Disc System Outputs to Gray Wedge Input.

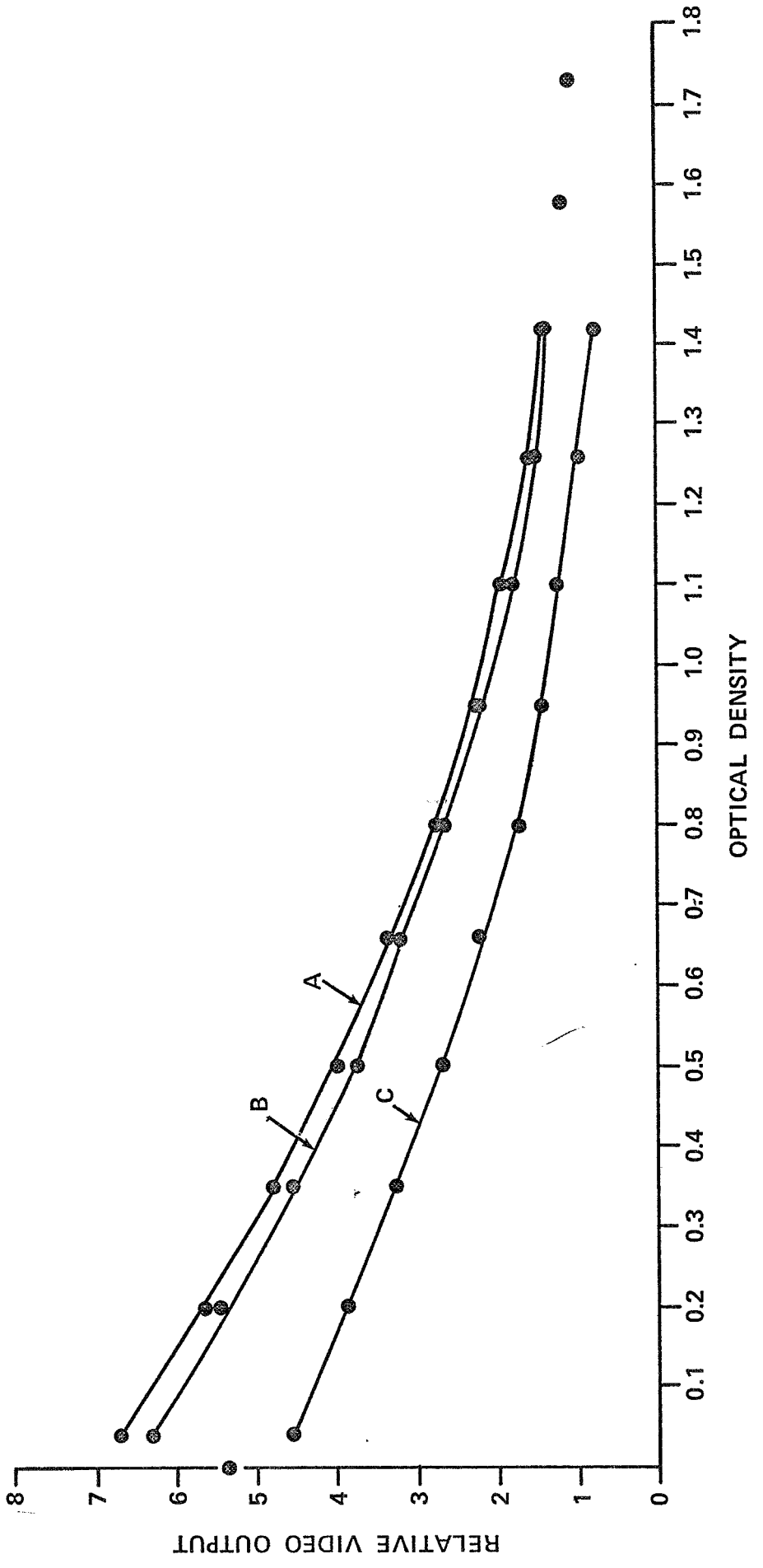
RELATIVE VIDEO OUTPUT
OPTICAL DENSITY
0
1
2
3
4
5
6
7
8
0.1
0.2
0.3
0.4
0.5
0.6
0.7
0.8
0.9
1.0
1.1
1.2
1.3
1.4
1.5
1.6
1.7
1.8
A
B
C

FIG. 11: Test Circuit for Pulsing of Light Source.

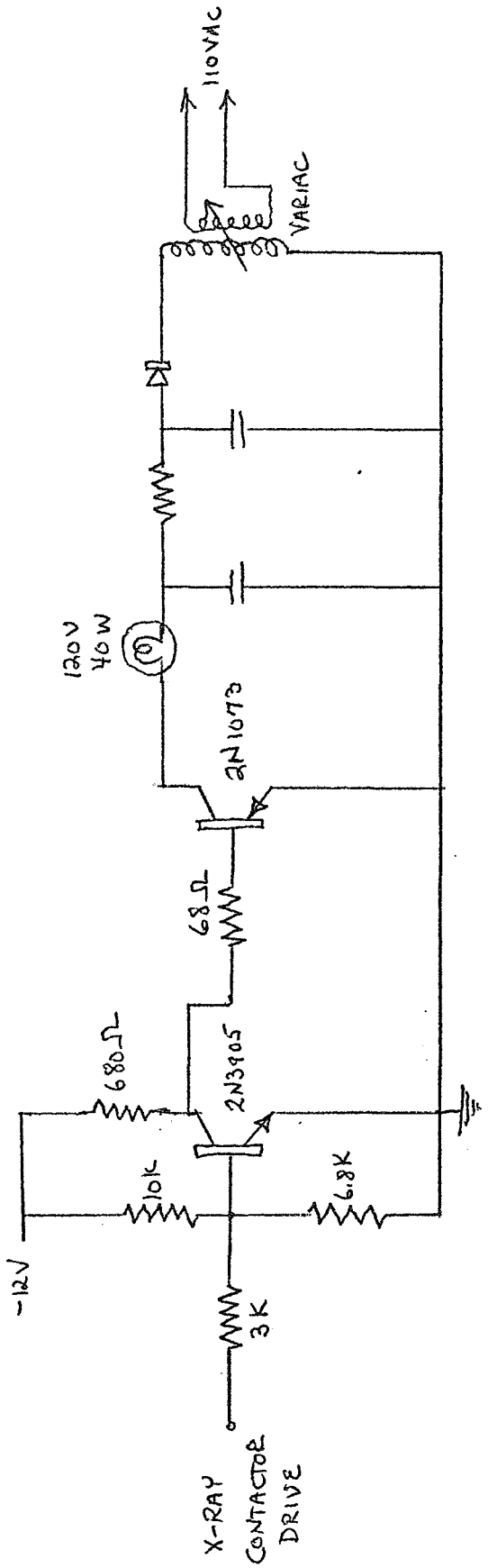

40 WATT LIGHT PULSE DRIVE CIRCUIT

used in the input video amplifier of the disc was reduced thereby reducing the bandwidth of the input amplifier but also reducing distortion of the usable signal.

The MTF of the TV camera-video disc combination was determined by exposing a moist bar pattern to the TV camera whose bars have a varying spatial frequency. The spacing between the bars and their thickness varies logarithmically between groups. A single horizontal scan line of composite video, taken normal to the direction of the bars, was photographed and the relative response as a function of spatial frequency was determined.

Figs. 5 and 6 represent a single line of composite video at the TV camera and video disc outputs for the Moiré pattern input, and normal double field scan. Fig. 7 shows the resulting MTF for the TV camera and disc combination.

Using an Eastman Kodak calibrated step wedge, the gray level response of the TV camera and video disc combination in the normal double-field scan mode was determined. The gray level response was tested by placing the step wedge using a horizontal position and on the surface of a standard roentgenographic viewbox. One horizontal line of composite video was photographed, and the relative video output voltage across this line was measured. This was plotted against the optical density corresponding to each step of the wedge. Fig. 8 is the TV camera response to the step wedge, while Fig. 9 is the video disc response (in the playback mode). Fig. 10 shows the relative responses of the TV camera, disc-electronics, and the disc output for the data recorded in Fig. 9.

Determination of the MTF of the TV camera - video disc combination in the single-scan mode was accomplished in essentially the same manner as in the double field scan mode, except that the illumination for the pattern was provided by pulsing a 40 watt incandescent bulb. The x-ray contactor pulse from the single-scan control box provided the signal to drive the circuit shown in Fig. 11. The 40 watt lamp was enclosed in the housing of a standard roentgenographic viewbox to provide a uniform diffusing surface. The Moiré pattern was placed upon the surface of the roentgenographic viewbox, using the same distance from lens to pattern as for previous

FIG. 12: Composite Video Signal (single horizontal line) for Complete System Operated in the Single-Scan Mode. Input was the Moiré Pattern.

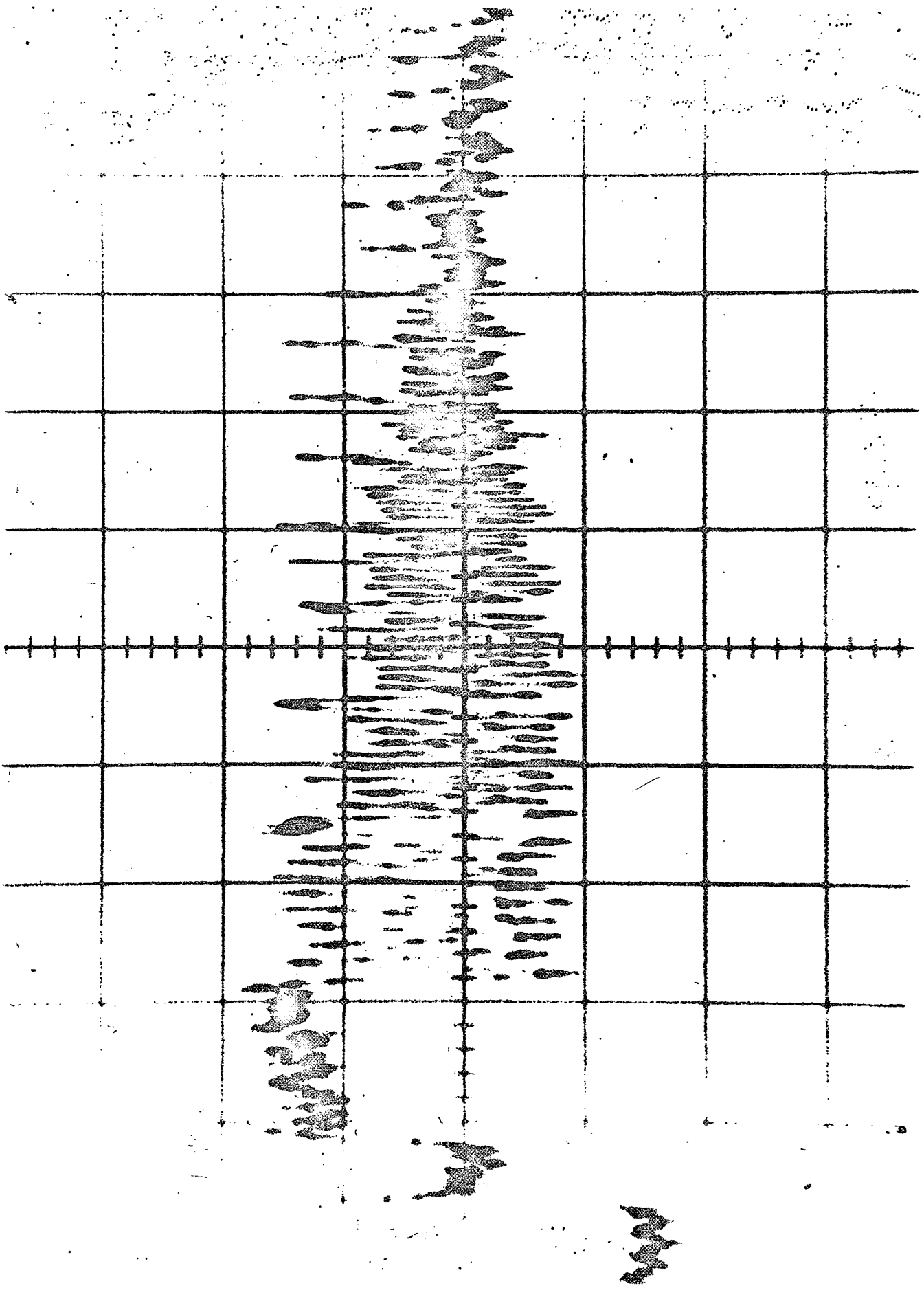

FIG. 13: Modulation Transfer Function of the Moiré Pattern. System Operated in the Single-Scan Mode.

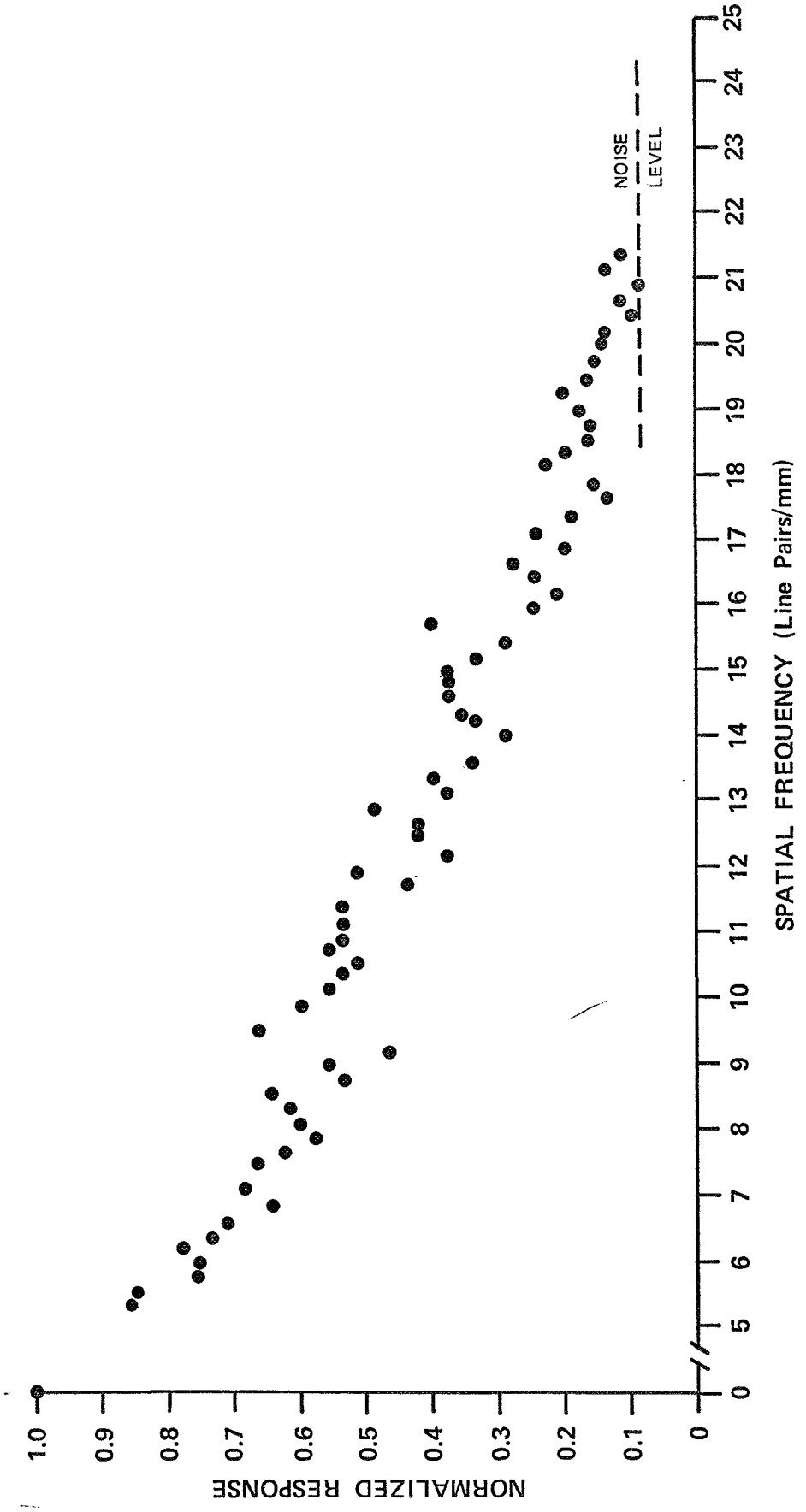
NORMALIZED RESPONSE
1.0
0.9
0.8
0.7
0.6
0.5
0.4
0.3
0.2
0.1
0
0
5
6
7
8
9
10
11
12
13
14
15
16
17
18
19
20
21
22
23
24
25
SPATIAL FREQUENCY (Line Pairs/mm)
NOISE
LEVEL

FIG. 14: Video Converter Output for one Vertical Scan.

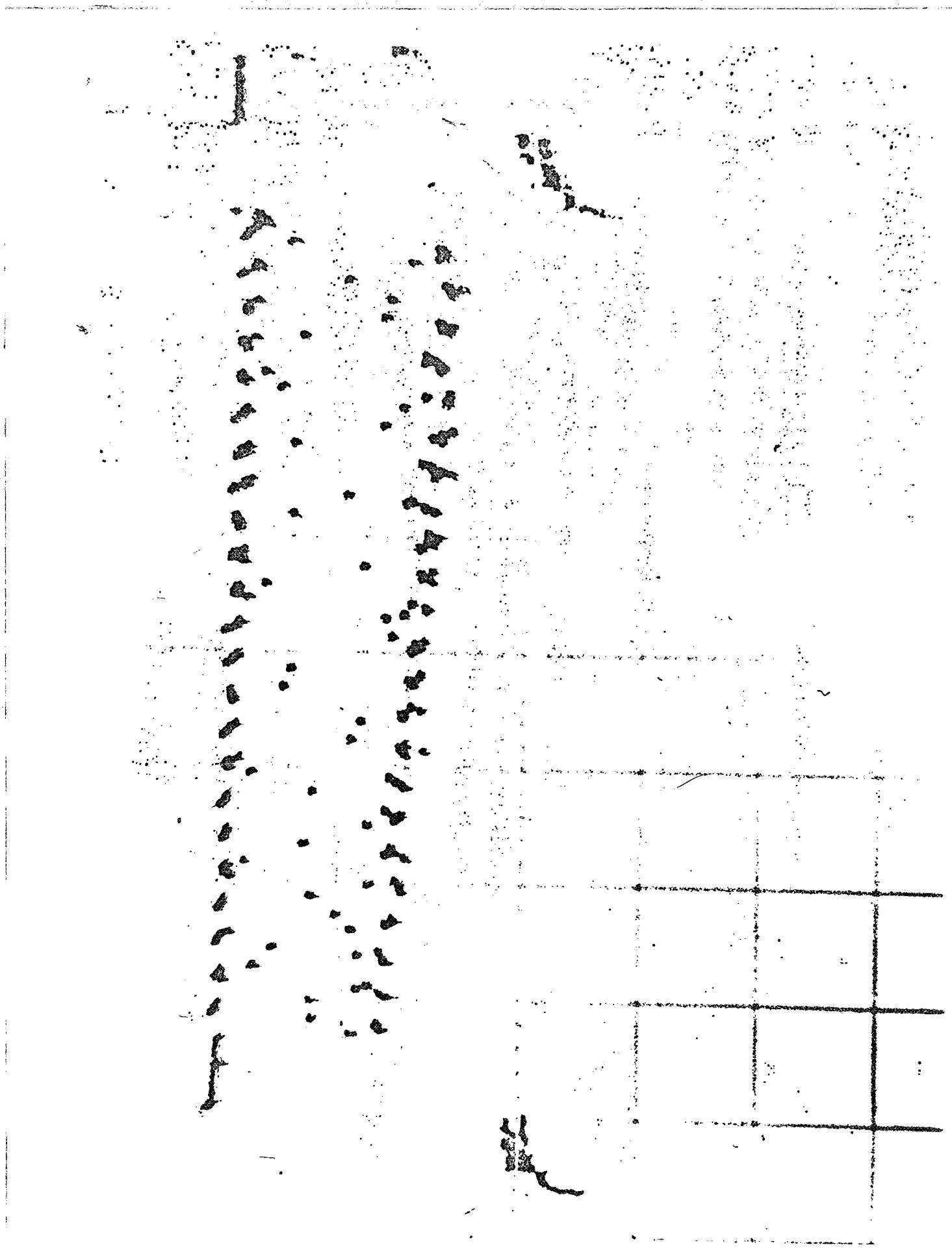

FIG. 15: Distance from first pulse representing a horizontal bar to successive pulses (additional bars of test pattern) -vs- bar number.

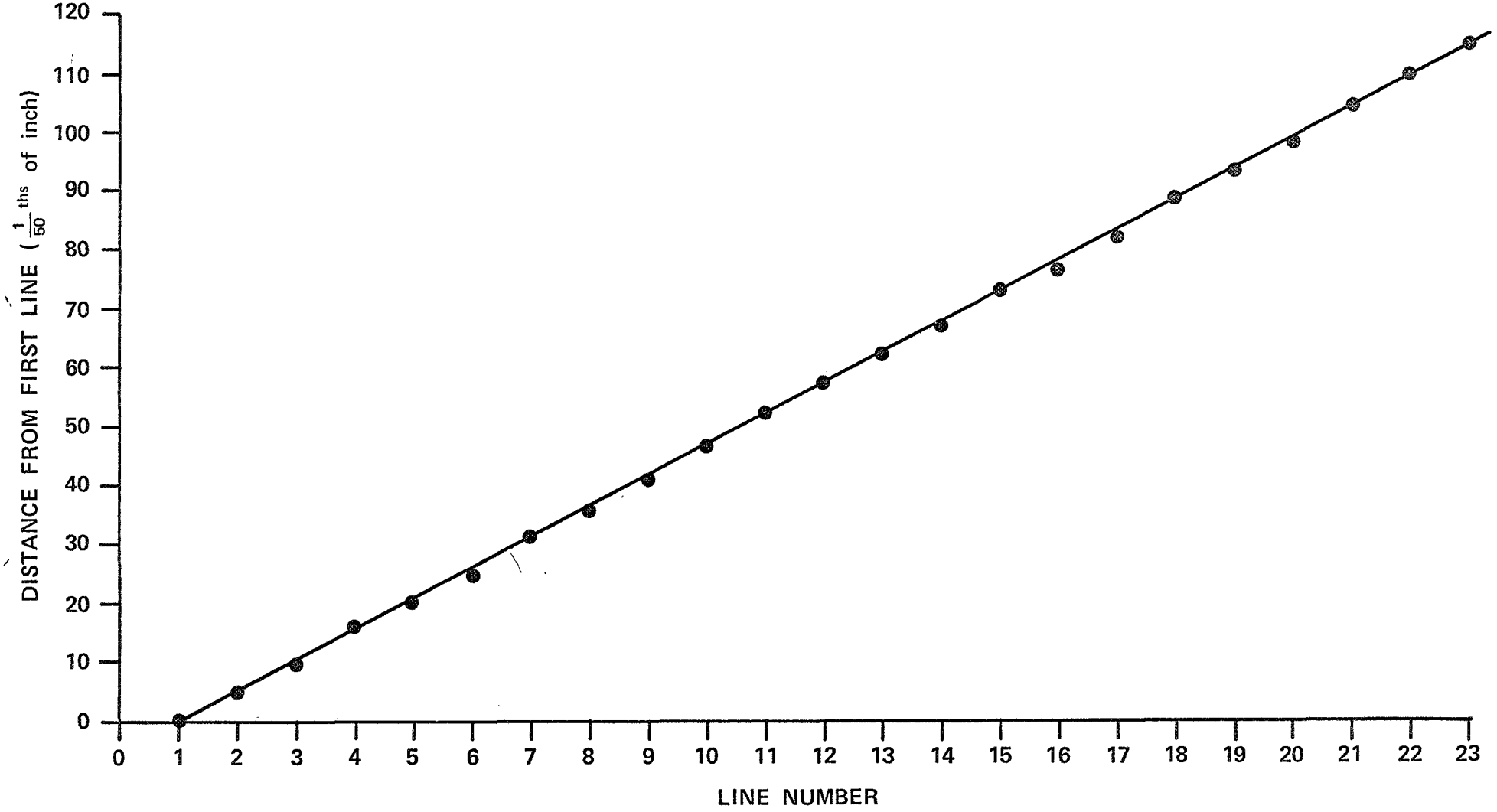
DISTANCE FROM FIRST LINE ($\frac{1}{50}$ths of inch)
120
110
100
90
80
70
60
50
40
30
20
10
0
0 1 2 3 4 5 6 7 8 9 10 11 12 13 14 15 16 17 18 19 20 21 22 23
LINE NUMBER

FIG. 16: Linearity of Horizontal Scan (of video converter) -vs- Time as a Function of Scan Rate.

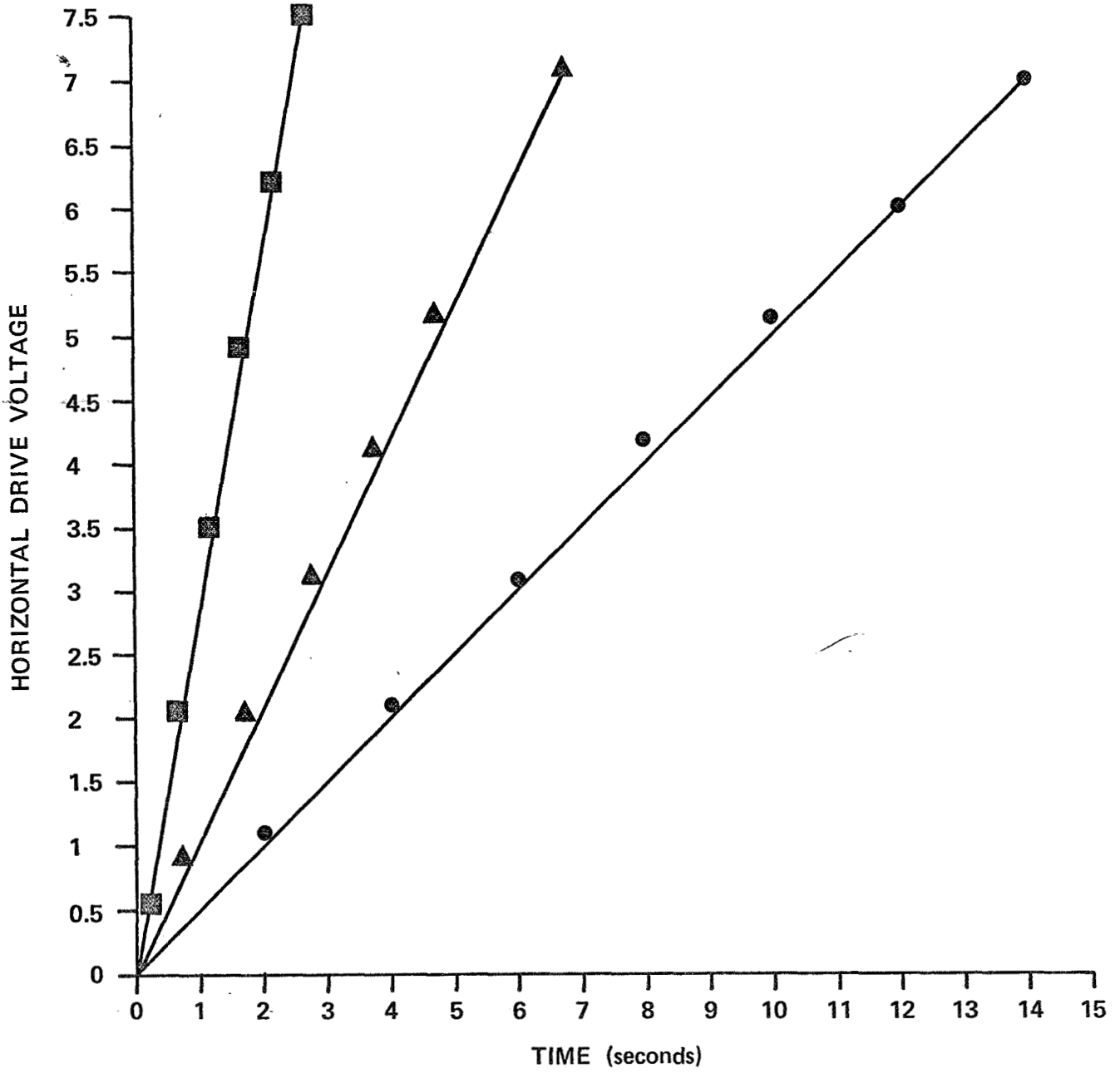
HORIZONTAL DRIVE VOLTAGE
7.5
7
6.5
6
5.5
5
4.5
4
3.5
3
2.5
2
1.5
1
0.5
0
0 1 2 3 4 5 6 7 8 9 10 11 12 13 14 15
TIME (seconds)

FIG. 17: Block Diagram of Complete Digitized Single-Scan Video - X-Ray System.

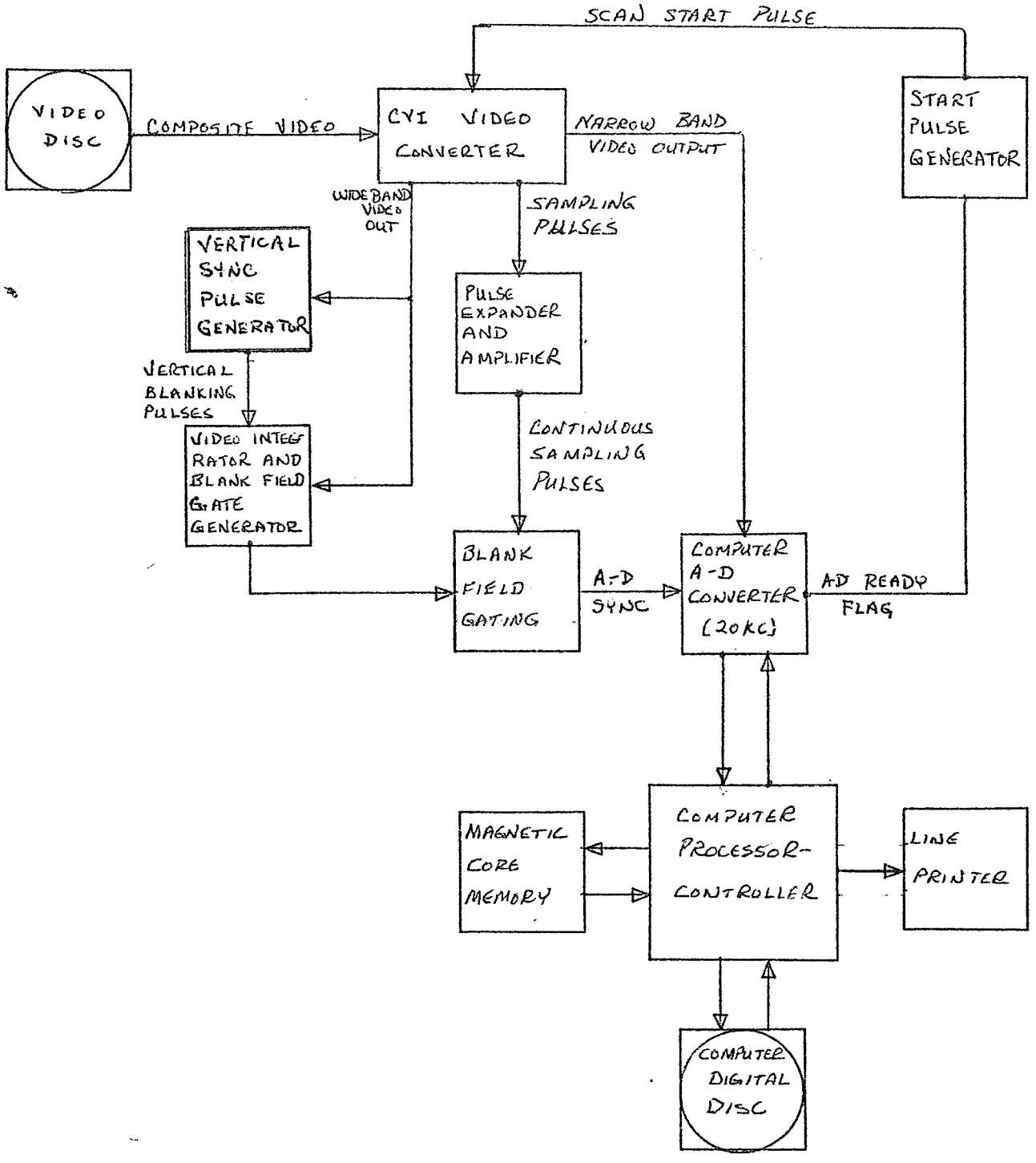

MVR VIDEO DISC – IBM 1801 COMPUTER PICTURE PROCESSING SYSTEM DIAGRAM

measurements. Fig. 12 shows one horizontal line of the composite video signal for the Moire pattern. Fig. 13 shows the MTF. As can be seen in Fig. 13, the MTF approaches the 0.10 level at a spatial frequency of 21 line pairs per millimeter at the vidicon face. This represents a spatial frequency of 3 line pairs per millimeter at the front surface of a seven inch image intensifier.

Tests have also been run to determine the linearity of the CVI video converter. Two linearity criteria were tested: first, the linearity of the vertical scan and second, the linearity of the horizontal scan. (Here, vertical and horizontal are referenced to the sequence of picture points scanned relative to the TV raster.)

The vertical scan linearity test involved scanning a pattern of uniformly spaced horizontal black bars with the TV camera, recording the video converter output for one vertical scan on a storage oscilloscope. This pattern was then photographed (Fig. 14) and the distance from the first pulse representing a bar to each successive pulse was measured. These distances were plotted against the bar number and is shown in Fig. 15. The linearity of the sweep is readily apparent.

The linearity of the horizontal scan of the video converter was determined by photographing the horizontal sweep ramp as generated by the video converter. Fig. 16 shows the plots of this ramp for three different scan rates. Here, a non-linearity is evident, but it is less than 3% and should, therefore, not introduce a significant distribution of the digital data.

In an effort to gain some insight into the factors involved in computerizing single-scan TV pictures, an attempt was made to interface the MVR video disc to an IBM 1801 computer. The computer system used was a 2 μs cycle time IBM 1801 computer with time sharing executive assembler and a 1810 disc storage system, analog-to-digital (A-D) converter and a line printer comparable to the IBM 1443 line printer.

Fig. 17 is a block diagram of the video disc computer picture processing system developed. The CVI video converter was used to generate a narrow band video signal capable

FIG. 18: Pulse Stretcher for Scan Converter Output.

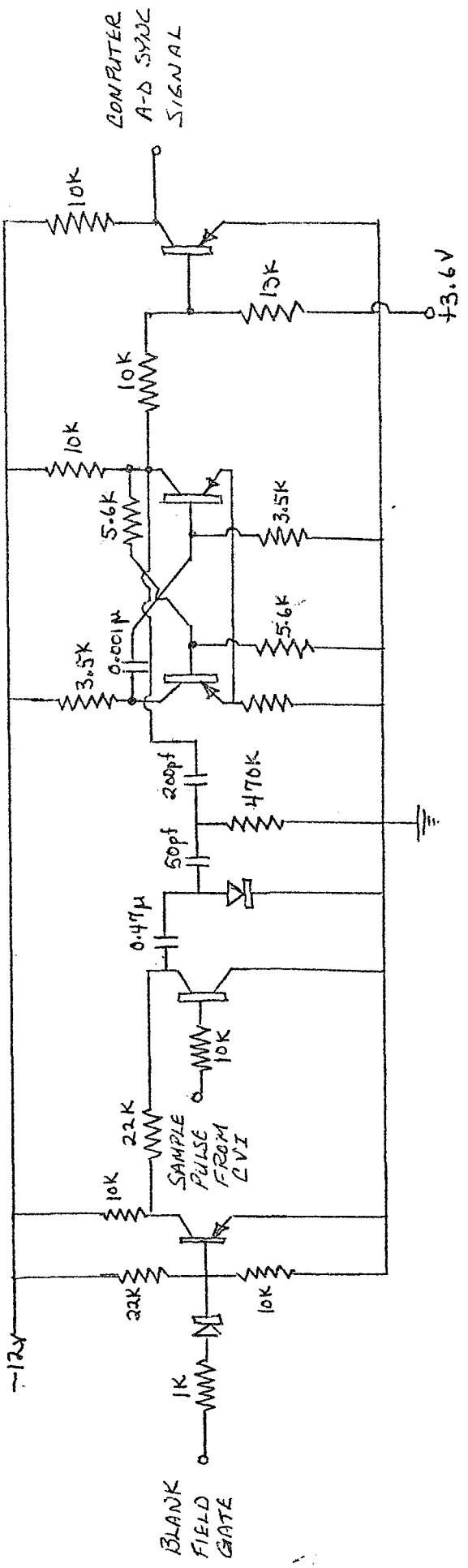

1. All Transistors are 2N3905
2. All Diodes are 2N4002

COMPUTER A–D SYNC GENERATING CIRCUIT

FIG. 19: Vertical Synchronization Pulse Generator.

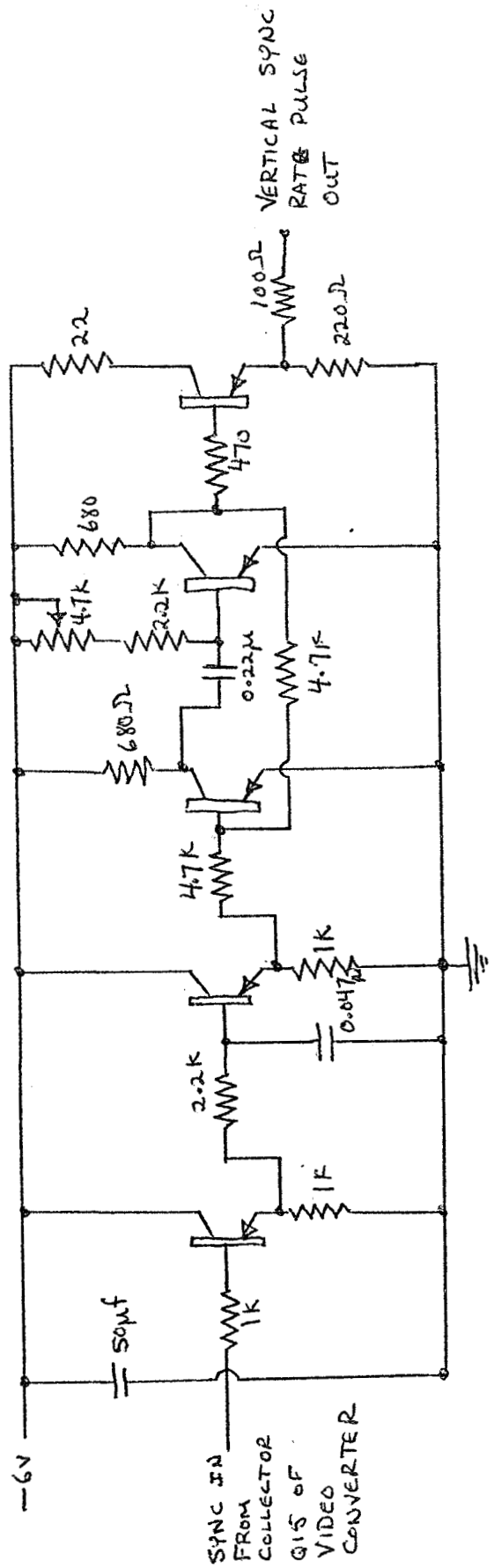

1. ALL Transistors are 2N3638

VERTICAL SYNC RATE PULSE GENERATOR

FIG. 20: Blank Field Gate Generating Circuit.

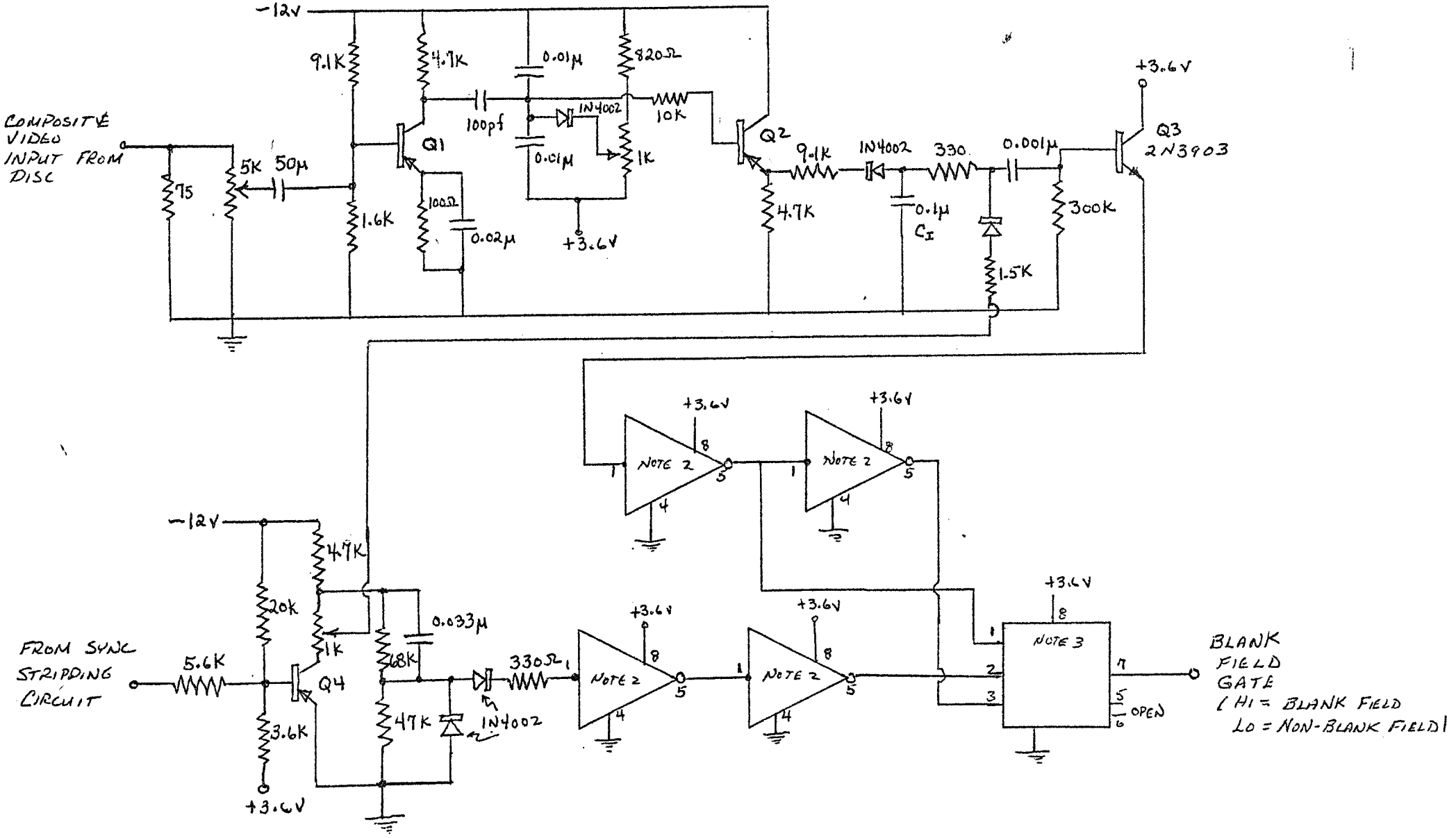

BLANK FIELD GATE GENERATING CIRCUIT

1. All PNP Transistors are 2N3905
2. Triangles are Buffer Amplifiers — Motorola integrated circuits MC 700 G
3. Box is J–K Flip flop IC

FIG. 21: Start Pulse Generator Circuit.

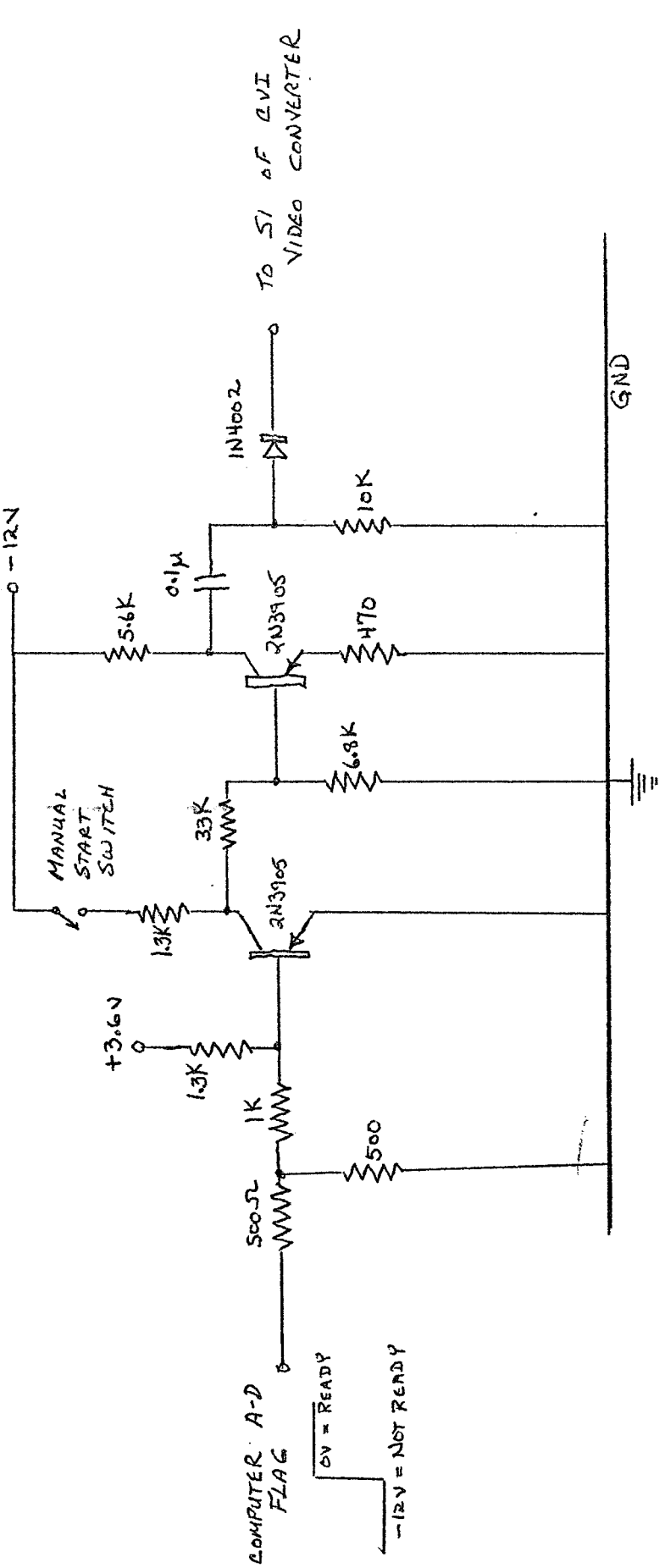

START PULSE GENERATING CIRCUIT

FIG. 22: Computer Program Schematic.

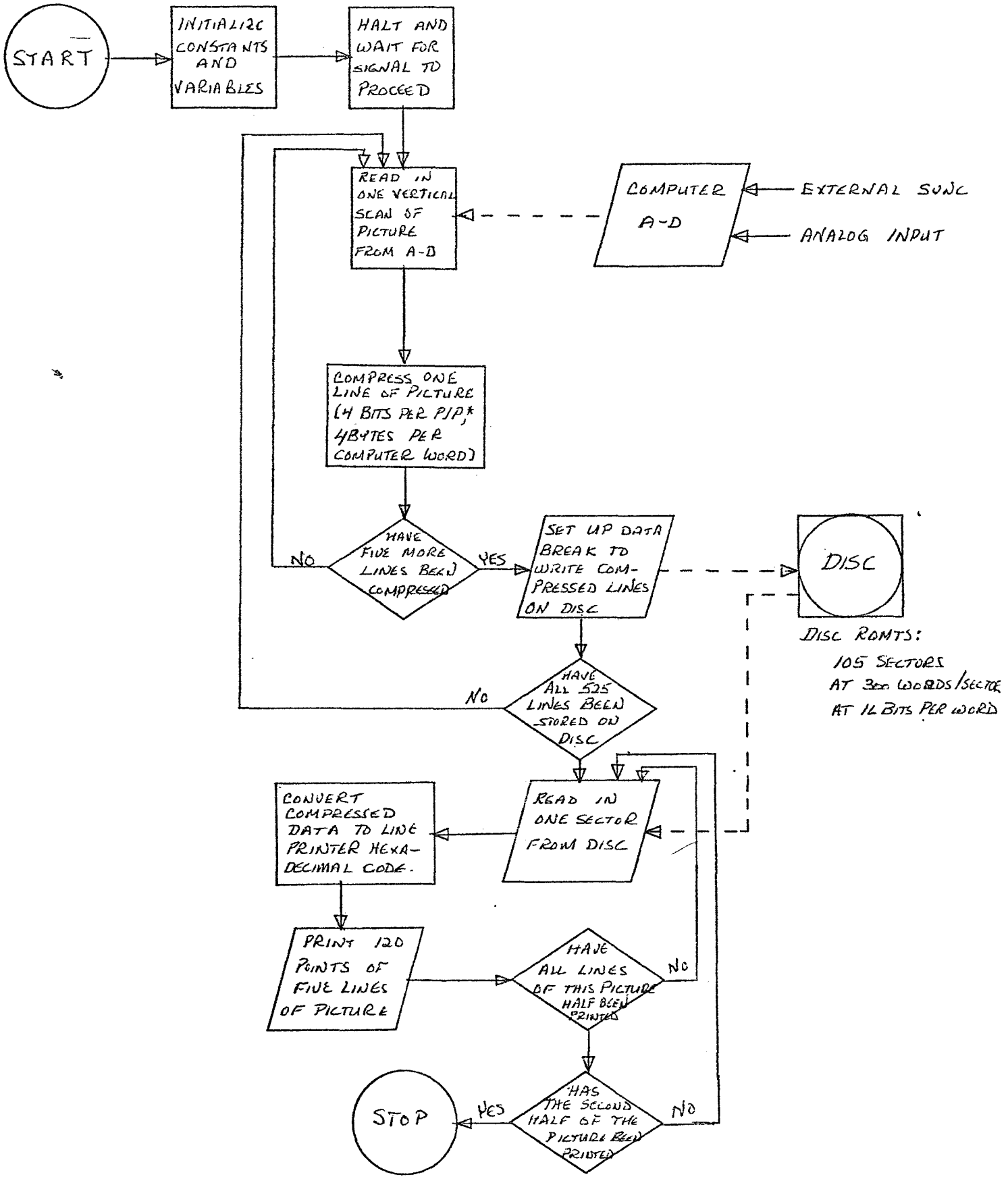

IBM 1801 COMPUTER PROGRAM BLOCK DIAGRAM —

Program converts analog input from video disc into a hexa-decimal digitalized picture.

of being handled by the A-D converter of the computer. This A-D could accommodate a 20 KC input rate. In order to ensure proper synchronization of the A-D converter and the video scanner the sampling pulses from the video converter were used to generate sync pulses to drive the A-D sync line. Fig. 18 shows the circuit used to lengthen the video converter sample pulses to the 5 μs pulse width required by the computer. Additionally, it was necessary to gate off the A-D converter sync pulses during the periods when the video converter scanned the blank fields of the single-scan picture. This gating served the dual purpose of preventing meaningless blank field information from being processed by the computer, and also provided the 16 milliseconds blank field time during which the computer processed the previous block of information.

The vertical sync pulse generator circuit shown in Fig. 19 was used to provide a synchronizing signal to the blank field gate generating circuit of Fig. 20. In the blank field gate generating circuit, transistors Q1 and Q2 amplify and set the DC level of a composite video signal which is integrated over 16 millisecond periods by C_I. Transistors Q3 and Q4 provide a discharge and detection circuit for the charge that is stored in C_I. During a blank field input, the charge on C_I remains essentially unchanged, while during a non-blank field input, C_I develops a voltage acrossed it which is detected and after amplification used to set the appropriate state of the output of the J-K flip-flop.

The start pulse generator circuit of Fig. 21 detects the zero level "ready" signal provided by the A-D converter in the computer. When this signal is received, a pulse is sent to the video converter which initiates its scanning. A manual start switch is also provided which can be used to start the scan manually any time after the computer A-D converter flag goes to zero.

A block diagram of the program used to process the single-scan TV picture in the computer is shown in Fig. 22. This program consists of two chronological subprograms: the

single-scan TV picture read-in to the digital disc and the transfer of the picture from the digital disc to the output device. The program was written in IBM 1801 TSX assembly language. This program is available on request.

In the read-in subprogram, the computer reads in and digitalizes each picture point of each vertical scan in accordance with the sync signals to the A-D converter. After receiving the 240 picture points of each vertical scan (in 16 milliseconds), the computer compresses this data and stores it in an output table. The digitalized picture points are coded in 11 bit words which are then truncated to the four most significant bits and used to form a byte. These bytes are then stored four to a 16 bit computer word in the output table. Each vertical line therefore requires 60 computer words in the output table. As each IBM 1810 disc sector is 320 words long and the smallest increment of disc is one sector, the output tables were 300 computer words in length and represent five picture scan lines. Each time one of the three output tables becomes filled, a data breakline between that table and the digital disc is activated. On a cycle steal basis, the output table is transferred to a sector on the disc. After each vertical line of scan of the picture is compressed, if the output table is not full, the computer waits for the next line of scan. The compression and storage of a single-scan line requires about 5.5 milliseconds of computer time.

Upon completing the storage of a digitalized single-scan TV picture on the disc, the computer reads-in the sectors of the disc in reverse order to which they were written. After each disc sector is read-in, the bytes for the first half of each line scanned on the picture are sequentially picked out, encoded in the format for the line printer, and printed out at 120 picture points per line printer line. After the top half of the picture has been printed, the above process is repeated for the bottom half of the picture. The resulting picture is in sixteen gray levels represented in hexadecimal code; i.e., 0-9, A, B, C, D, E, F with 0 being the darkest part of the picture and F the lightest.

As has been stated, the completed tests were run on an IBM 1801 computer. Future picture processing work is expected to be done on a PDP-8E minicomputer. The IBM 1801

computer offers the advantages of a 32K word memory and a large and flexible instruction set. The 8K memory capability of the PDP-8E will be sufficient, despite the fact that the PDP-8E has a 12 bit word as the program written for the IBM 1801 used less than four thousand words, most of which were reserved for tables. The limited instruction set of the PDP-8E will be a handicap but will in part be offset by the decreased memory cycle time of the PDP-8E as compared to the IBM 1801; i.e., 0.6 μs vice 2.0 μs.

PUBLICATIONS DURING THIS PERIOD

1. Microdosimetry of Charged Particles in Low Atomic Number Materials: N.A.Baily, J.E.Steigerwalt, and J.W.Hilbert, Radiology 94, 196 (1970).

2. Frequency Distributions of Energy Deposition by Fast Charged Particles: N.A.Baily, J.E.Steigerwalt, and J.W.Hilbert, Phys. Rev. 2, B, 577 (1970).

3. Measurements of the Frequency Distributions of Small Energy Losses by 46.4 MeV Protons and Theoretical Predictions Using the Method of Kellerer: J.E.Steigerwalt, N.A.Baily, and J.W.Hilbert, Rad. Res. 43, 234 (1970).

4. Frequency Distributions of the Magnitude of Energy Transfers from High Energy Protons to Tissue Equivalent Materials: N.A.Baily, J.E.Steigerwalt, and J.W.Hilbert, Proceedings of the IV International Congress of Radiation Research, 14 (1970).

PERSONNEL PARTICIPATING IN PROGRAM

1. Norman A. Baily, Professor of Radiology
2. John E. Steigerwalt, Assistant Radiation Research Physicist
3. Ronald L. Crepeau, Assistant Developmental Engineer
4. Arthur E. Loomis, Laboratory Technician
5. Jerald W. Hilbert, Supervising Hospital Radiation Physicist